

# REFINE: Residual Feature Integration is Sufficient to Prevent Negative Transfer

Yichen Xu<sup>1</sup>, Ryumei Nakada<sup>2</sup>, Linjun Zhang<sup>\*3</sup>, and Lexin Li<sup>\*4</sup>

<sup>1</sup>University of California, Berkeley. Email: yichen\_xu@berkeley.edu   <sup>2</sup>Rutgers University. Email: rn375@rutgers.edu   <sup>3</sup>Rutgers University. Email: lz412@stat.rutgers.edu   <sup>4</sup>University of California, Berkeley. Email: lexinli@berkeley.edu

## Abstract

Transfer learning typically leverages representations learned from a source domain to improve performance on a target task. A common approach is to extract features from a pre-trained model and directly apply them for target prediction. However, this strategy is prone to negative transfer where the source representation fails to align with the target distribution. In this article, we propose Residual Feature Integration (REFINE), a simple yet effective method designed to mitigate negative transfer. Our approach combines a fixed source-side representation with a trainable target-side encoder and fits a shallow neural network on the resulting joint representation, which adapts to the target domain while preserving transferable knowledge from the source domain. Theoretically, we prove that REFINE is sufficient to prevent negative transfer under mild conditions, and derive the generalization bound demonstrating its theoretical benefit. Empirically, we show that REFINE consistently enhances performance across diverse application and data modalities including vision, text, and tabular data, and outperforms numerous alternative solutions. Our method is lightweight, architecture-agnostic, and robust, making it a valuable addition to the existing transfer learning toolbox.

## 1 Introduction

Transfer learning provides a fundamental paradigm in modern machine learning, where knowledge acquired from one task (source domain) is leveraged to enhance performance on another related task (target domain). It encompasses a wide range of applications, from adapting models across different sources or domains, to distilling knowledge from large, pre-trained models into smaller, task-specific models. Despite its success, however, it faces the challenge of negative transfer, where the transferred representation does not align with the target distribution, resulting in degraded rather than improved performance. Negative transfer can arise due to numerous reasons, including label noise, semantic confusion, or class imbalance, leading to a misalignment between the source knowledge and the target requirement. Effective transfer learning therefore requires careful strategy design and robust mechanisms to mitigate the risks of negative transfer (Zhang et al., 2023).

In this article, we develop a simple yet effective approach to mitigate negative transfer. Our key idea is that, after obtaining the transferred representation  $f_{\text{rep}}(x)$  from the source

---

\*co-corresponding author

domain, instead of relying solely on  $f_{\text{rep}}(x)$ , we further introduce a residual connection with a trainable feature encoder  $h(x)$  that is learned from the target domain. We then combine  $f_{\text{rep}}(x)$  and  $h(x)$ , and fit a shallow neural network on the concatenated representation  $(f_{\text{rep}}(x), h(x))$ . Intuitively, while  $f_{\text{rep}}(x)$  captures transferable features, it may omit target-specific signals that are critical for accurate prediction in the target domain. The residual connection via  $h(x)$  compensates for this omission, ensuring that essential information in the target domain is preserved. Furthermore, because  $f_{\text{rep}}(x)$  already encodes a substantial portion of the predictive signal, learning from the joint representation  $(f_{\text{rep}}(x), h(x))$  can potentially be achieved with a much simpler class of functions than learning from  $x$  or  $h(x)$  alone. We demonstrate, both theoretically and empirically, that this strategy is *sufficient to prevent negative transfer* across a broad range of settings. Conceptually, our method follows a similar spirit as the seminal deep residual learning (ResNet) of He et al. (2016), and thus we call our method *Residual Feature Integration* (REFINE). Figure 1 gives a schematic overview of our method.

Our contributions are threefold. First, it offers a lightweight and broadly applicable enhancement to existing transfer learning pipelines. Unlike the methods that require re-training of the entire model or domain adaptation that explicitly aligns distributions,

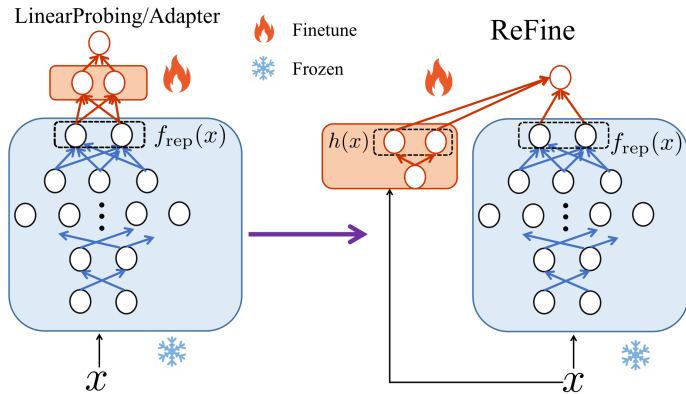


Figure 1: A schematic overview of REFINe.

our approach is easy to train with minimal computational overhead, is architecture-agnostic, and is robust across a variety of applications and data modalities. Second, we formally justify this simple yet effective method through a rigorous theoretical analysis, which constitutes a key contribution of this article. Specifically, we show that augmenting any frozen  $f_{\text{rep}}$  with a trainable  $h(x)$  guarantees that the resulting predictor achieves a convergence rate of prediction risk that is never worse than that obtained by training from scratch on the target data alone. In other words, REFINe is inherently robust against negative transfer in the worst-case scenario. Moreover, our prediction risk bound seamlessly transitions from the non-parametric convergence rate to a better near-parametric rate when the residual signal becomes sufficiently helpful. Finally, we carry out extensive numerical experiments on a variety of benchmark datasets, spanning vision, text, and tabular data, and also compare with a number of alternative solutions. We empirically verify that our approach effectively mitigates negative transfer, in particular when there is significant representational mismatch or task divergence.<sup>1</sup>

## 2 Related Works

**Transfer learning.** Linear probing (Kumar et al., 2022), and adapter-based feature extraction (Houlsby et al., 2019) are probably two of the most widely used transfer learning approaches. Both methods operate by extracting the penultimate layer of features from a pre-trained model in the source domain, followed by fine-tuning the last layer using the

<sup>1</sup>Our code is available at <https://github.com/Yyc-arch/ReFine.git>

data in the target domain. The main difference is that linear probing fits a linear layer for classification tasks, while the adapter-based method fits a shallow neural network. Both methods are computationally efficient, but are vulnerable to negative transfer. To mitigate negative transfer, various solutions have been proposed, often relying on an estimated similarity measure between the source and target domains (Gretton et al., 2012; Lin and Jung, 2017). However, in many practical applications, such similarity may be difficult to quantify, and some specific loss functions or architectures have to be imposed, which in turn limits the applicability of those solutions (Hosna et al., 2022). Alternatively, one may opt to fine-tune all layers of the model, but this incurs a substantial computational burden.

**Knowledge distillation.** Distillation is a technique in which a large, pre-trained model (teacher) transfers its knowledge to a smaller, more efficient model (student) (Hinton et al., 2015). As a form of transfer learning, knowledge distillation enables the student model to learn from the teacher’s predictions or intermediate representations, allowing it to achieve comparable performance with reduced complexity. However, distillation is also susceptible to negative transfer, particularly when the teacher model is misaligned with the target domain or when the knowledge it conveys is overly complex for the student model to effectively learn (Gou et al., 2021).

**Data augmentation.** Augmentation methods, such as deep generative models (Bowles et al., 2018; Anaby-Tavor et al., 2019) and statistical generation techniques Smyl and Kuber (2016), expand training data by creating additional samples. These methods, following scaling laws, aim to improve model performance through increased sample size (Jain et al., 2024). However, they are prone to distribution shifts or label corruption Nguyen et al. (2023); Compton et al. (2023); Lin et al. (2022); Jha et al. (2020), which can degrade model performance. In contrast, our approach goes beyond traditional data augmentation, by safely leveraging representations from an external model to enhance classifiers trained on small datasets.

**Stacking, adapters, and residual learning.** Stacking is an ensemble learning technique that combines the predictions of multiple base models by training a meta-learner on their outputs with a validation dataset. This approach is generally more robust than simple averaging (Cheng Ju and van der Laan, 2018), which can fail if even one base model is weak (Mohammed and Kora, 2023). Many existing ensemble transfer methods, however, assume that the external models are reliable and are trained on the same, potentially flawed, dataset (Ghorbani and Zou, 2019; Grover et al., 2023; Li et al., 2021). Moreover, stacking requires the base models to share aligned output spaces, which limits its applicability across tasks. Adapters are lightweight, trainable modules inserted into pre-trained models to enable domain adaptation without modifying the original model’s weights. They operate by leveraging the fixed features of the pre-trained model, but their effectiveness is limited when these features are misaligned with the target domain. Finally, although the concept of residual learning is widely used in methods such as ResNet (He et al., 2016) and gradient boosting (Ke et al., 2017), its potential for mitigating negative transfer remains under-explored.

### 3 Problem Formulation and Algorithm

Transfer learning aims to leverage knowledge from a source task to improve performance on a related target task. A common practice is to use a representation function  $f_{\text{rep}}$  learned from a large source dataset  $D_s$  under a source distribution  $\mathcal{P}_s$  as an extracted feature for the target task. However, if  $f_{\text{rep}}$  does not align well with the target distribution  $\mathcal{P}_t$ , naively reusing it can lead to negative transfer, resulting in degraded performance compared to

---

**Algorithm 1** The residual feature integration (REFINE) method.

---

- 1: **Input:** Training data  $\mathcal{D}_{\text{train}} = (x_i, y_i)_i$ , test data  $\mathcal{D}_{\text{test}}$ , pre-trained model  $f$ , loss function  $\ell$ .
  - 2: **Output:** Prediction of the label  $\hat{y}(x_0)$  for  $x_0 \in \mathcal{D}_{\text{test}}$ .
  - 3: **Training Phase:**
  - 4:     (a) Extract  $f_{\text{rep}}(x)$  from the penultimate-layer of a frozen pre-trained model  $f$ .
  - 5:     (b) Construct the concatenated features  $C_h(x) = (f_{\text{rep}}(x), h(x))$ .
  - 6:     (c) Let  $(\hat{w}, \hat{h})$  be the minimizer of  $\sum_i \ell(w(C_h(X_i)), Y_i)$  while freezing  $f_{\text{rep}}$ .
  - 7: **Prediction Phase:**
  - 8:     (a) Compute  $C_h(x_0)$  with the frozen  $f$ .
  - 9:     (b) Obtain the final prediction  $\hat{y}(x_0)$  based on  $\hat{w}(C_{\hat{h}}(x_0))$ .
- 

using the target data alone.

We formalize the Residual Feature Integration (REFINE) approach. The objective is to construct a method such that, when  $f_{\text{rep}}$  aligns well with the target distribution, effectively leverage transferred knowledge and outperform models trained from scratch on target data only, and when  $f_{\text{rep}}$  misaligns with the target distribution, safeguard against negative transfer and outperform models that rely solely on  $f_{\text{rep}}(x)$ .

We focus on the classification task as an illustration. Let  $D_t = \{(x_i, y_i)\}_{i=1}^n \sim \mathcal{P}_t$  denote the labeled dataset from the target task. Assume the access to a frozen extracted feature  $f_{\text{rep}} : \mathcal{X} \rightarrow \mathbb{R}^p$  trained on an external source data  $D_s$ . Define a class  $\mathcal{H}$  of trainable feature encoders  $h : \mathcal{X} \rightarrow \mathbb{R}^q$  and a class  $\mathcal{W}$  of trainable adapters  $w : \mathbb{R}^{p+q} \rightarrow \mathbb{R}^k$  on top of  $(f_{\text{rep}}(x), h(x))$ . Let  $w_{\text{ft}}$  be the trained adapter on top of the baseline model, and let  $g_{\text{sc}}$  be the model trained from scratch on  $x$ . We seek to learn both the encoder  $h$  and the adapter  $w$ , such that

$$\mathcal{R}_{\mathcal{P}_t}(w \circ (f_{\text{rep}}, h)) \leq \min\{\mathcal{R}_{\mathcal{P}_t}(w_{\text{ft}} \circ f_{\text{rep}}), \mathcal{R}_{\mathcal{P}_t}(g_{\text{sc}})\} \quad (1)$$

where  $\mathcal{R}_{\mathcal{P}}$  denotes the expected loss under the distribution  $\mathcal{P}$ .

Algorithm 1 outlines the REFINE approach. It extracts  $f_{\text{rep}}(x)$  from the penultimate-layer of a frozen pre-trained model, and combines it with the residual connection  $h(x)$ . The concatenated features  $(f_{\text{rep}}(x), h(x))$  are passed to a linear classifier for prediction, where only  $h(x)$  and the adapter  $w$  are updated, whereas the pre-trained model and  $f_{\text{rep}}(x)$  remain unchanged. This design allows REFINE to efficiently leverage transferred knowledge while adapting to the new task with minimal additional computation.

## 4 Numerical Experiments

### 4.1 Experiment setup

We evaluate the empirical performance of REFINE across various scenarios prone to negative transfer, including heavy label noise, semantic confusion, and class imbalance. We consider benchmark datasets across diverse application and data modalities of vision, text, and tabular, including CIFAR-10, CIFAR-100 Krizhevsky (2009), STL (Coates et al., 2011), Clipart, Sketch (Peng et al., 2019), USPS, MNIST, Books, Kitchen, DVD, and Electronics (Blitzer et al., 2007). We also compare with a number of alternative solutions, including a no-transfer baseline (NoTrans), linear probing (LinearProb, Kumar et al., 2022), adapter (Adapter, Houlsby et al., 2019), and knowledge distillation (Distillation, Hinton et al., 2015). For distillation, we follow the vanilla setup of Hinton et al. (2015), training a student using a weighted combination of cross-entropy loss on the true labels and KL divergence on

temperature-scaled soft targets from a frozen teacher. We omit full fine-tuning of all model layers, as our focus is on feature reuse without assuming access to the full model or requiring extensive parameter updates. We evaluate the method performance using a set of criteria, including classification accuracy, area under ROC (AUC), F1 score, and minimum class accuracy. For the neural network architecture, We primarily focus on convolutional neural network (CNN), while we employ other architectures as well. Results based on transformers are presented in Appendix C and in Table 5, which covers text-based tasks. We consider three settings: single-source transfer under heavy label noise, semantic confusion, and class imbalance, single-source transfer with potential distribution shift, and multi-source transfer. All models are trained with stochastic gradient descent (SGD) using a learning rate of 0.01 and momentum 0.9, with pretraining for 60 epochs and fine-tuning for 30 epochs. More details about experiment setup are given in Appendix D. We also comment that REFINE can be parameter-efficient. For example, REFINE uses only 4.88% as many parameters as the frozen pretrained model, comparable to NoTransfer (4.68%), Distillation (4.68%), and Adapter (5.46%), and modestly higher than Linear Probe (0.20%) in all experiments on CIFAR.

## 4.2 Single-source transfer with noisy and imbalanced data

We first consider single-source transfer when the pretraining data is noisy, semantically perturbed, or imbalanced. We use CIFAR-10 and CIFAR-100, pretraining on 10,000 samples, fine-tuning on 4,000 samples, and evaluating on 10,000 testing samples. We simulate label noise by flipping 40% or 80% of labels, induce semantic confusion through paired-class flipping and additive image noise, and model data imbalance by resampling to a long-tailed distribution. In all these scenarios, REFINE consistently mitigates severe performance degradation and outperforms alternative solutions.

Table 1 reports the results under heavy label noise. With 40% label flips, REFINE outperforms the alternatives on both CIFAR-10 and CIFAR-100 in terms of accuracy, AUC, and F1 score, while maintaining a competitive minimum class accuracy. With more severe noise of 80% flips, Adapter and LinearProb collapse entirely. REFINE surpasses Adapter and LinearProb in accuracy by 38.10% and 37.12% on CIFAR-10, and by 16.37% on CIFAR-100, while maintains a comparable accuracy as NoTrans. REFINE also clearly outperforms Distillation across all scenarios.

Table 2 reports the results under semantic confusion. REFINE leads in terms of accuracy, F1 score, and minimum class accuracy, while falling slightly behind Distillation in AUC. Notably, LinearProb and Adapter fail to transfer effectively on CIFAR-10, with a degraded performance compared to NoTrans. In contrast, REFINE consistently improves all metrics on both CIFAR-10 and CIFAR-100.

Table 3 reports the results with data imbalance. For this scenario, on CIFAR-10, REFINE is the only method that maintains or slightly improves the performance over NoTrans, while LinearProb and Adapter degrade more severely than Distillation. On CIFAR-100, REFINE emerges as the most effective transfer method, followed by LinearProb and Adapter, with Distillation being the least effective. Also notably, on CIFAR-100, all baseline methods including LinearProb, Adapter, and Distillation suffer a zero minimum class accuracy, while REFINE manages to maintain a nonzero minimum class accuracy.

## 4.3 Single-source transfer with distribution shift

We next consider single-source transfer when there is potential distribution shift between the source and target domains. We consider the scenario of domain mismatch, including

Dataset	Flip Ratio	Model	Accuracy	AUC	F1	Min CAcc
CIFAR-10	40% flips	NoTrans	56.0480 $\pm$ 0.6377	0.9037 $\pm$ 0.0028	0.5580 $\pm$ 0.0080	32.4000 $\pm$ 5.8354
		LinearProb	65.5400 $\pm$ 0.0613	0.9378 $\pm$ 0.0003	0.6561 $\pm$ 0.0008	42.8200 $\pm$ 1.4483
		Adapter	65.7780 $\pm$ 0.1869	0.9376 $\pm$ 0.0007	0.6581 $\pm$ 0.0024	<b>45.2000 <math>\pm</math> 2.2865</b>
		Distillaton	57.0120 $\pm$ 0.5790	0.9115 $\pm$ 0.0016	0.5674 $\pm$ 0.0032	34.8400 $\pm$ 4.5275
		REFINE	<b>66.2280 <math>\pm</math> 0.3236</b>	<b>0.9388 <math>\pm</math> 0.0006</b>	<b>0.6625 <math>\pm</math> 0.0036</b>	43.9400 $\pm$ 3.7750
	80% flips	NoTrans	56.5740 $\pm$ 0.6416	0.9057 $\pm$ 0.0033	0.5622 $\pm$ 0.0055	33.6000 $\pm$ 3.0364
		LinearProb	19.4600 $\pm$ 0.7517	0.6895 $\pm$ 0.0011	0.1177 $\pm$ 0.0108	0.0000 $\pm$ 0.0000
		Adapter	18.4880 $\pm$ 0.4598	0.6906 $\pm$ 0.0006	0.1219 $\pm$ 0.0156	0.0000 $\pm$ 0.0000
		Distillaton	53.5100 $\pm$ 0.7910	0.8982 $\pm$ 0.0021	0.5269 $\pm$ 0.0091	26.8000 $\pm$ 2.4892
		REFINE	<b>56.5840 <math>\pm</math> 0.3258</b>	<b>0.9067 <math>\pm</math> 0.0019</b>	<b>0.5655 <math>\pm</math> 0.0041</b>	<b>36.9000 <math>\pm</math> 2.9353</b>
CIFAR-100	40% flips	NoTrans	17.8180 $\pm$ 0.3633	0.8259 $\pm$ 0.0068	0.1684 $\pm$ 0.0039	<b>0.6000 <math>\pm</math> 0.4899</b>
		LinearProb	17.3500 $\pm$ 0.2733	<b>0.8605 <math>\pm</math> 0.0015</b>	0.1472 $\pm$ 0.0043	0.0000 $\pm$ 0.0000
		Adapter	16.1900 $\pm$ 0.3272	0.8578 $\pm$ 0.0019	0.1303 $\pm$ 0.0037	0.0000 $\pm$ 0.0000
		Distillaton	18.7340 $\pm$ 0.2199	<b>0.8605 <math>\pm</math> 0.0035</b>	0.1631 $\pm$ 0.0024	0.0000 $\pm$ 0.0000
		REFINE	<b>19.2800 <math>\pm</math> 0.3362</b>	0.8555 $\pm$ 0.0042	<b>0.1805 <math>\pm</math> 0.0043</b>	0.4000 $\pm$ 0.8000
	80% flips	NoTrans	<b>17.5220 <math>\pm</math> 0.5970</b>	<b>0.8252 <math>\pm</math> 0.0059</b>	<b>0.1663 <math>\pm</math> 0.0047</b>	<b>0.6000 <math>\pm</math> 0.4899</b>
		LinearProb	1.0000 $\pm$ 0.0000	0.6740 $\pm$ 0.0019	0.0002 $\pm$ 0.0000	0.0000 $\pm$ 0.0000
		Adapter	1.0000 $\pm$ 0.0000	0.5250 $\pm$ 0.0058	0.0002 $\pm$ 0.0000	0.0000 $\pm$ 0.0000
		Distillaton	15.1060 $\pm$ 0.4869	0.8174 $\pm$ 0.0069	0.1227 $\pm$ 0.0039	0.0000 $\pm$ 0.0000
		REFINE	17.3700 $\pm$ 1.0922	0.8239 $\pm$ 0.0060	0.1641 $\pm$ 0.0109	0.2000 $\pm$ 0.4000

Table 1: Single-source transfer with heavy label noise using CNN.

Dataset	Model	Accuracy	AUC	F1	Min CAcc
CIFAR-10	NoTrans	56.5320 $\pm$ 0.7722	0.9006 $\pm$ 0.0021	0.5639 $\pm$ 0.0056	35.7600 $\pm$ 2.7507
	LinearProb	48.5420 $\pm$ 0.4246	0.8987 $\pm$ 0.0008	0.4757 $\pm$ 0.0046	18.4400 $\pm$ 7.8884
	Adapter	47.1740 $\pm$ 0.8231	0.8998 $\pm$ 0.0006	0.4479 $\pm$ 0.0148	7.4200 $\pm$ 6.4704
	Distillaton	57.7980 $\pm$ 0.4419	<b>0.9068 <math>\pm</math> 0.0009</b>	0.5772 $\pm$ 0.0037	35.9200 $\pm$ 3.0023
	REFINE	<b>58.6520 <math>\pm</math> 0.4685</b>	0.9034 $\pm$ 0.0011	<b>0.5861 <math>\pm</math> 0.0048</b>	<b>38.4000 <math>\pm</math> 3.1035</b>
	CIFAR-100	NoTrans	18.1280 $\pm$ 0.7416	0.8129 $\pm$ 0.0044	0.1747 $\pm$ 0.0073
LinearProb		20.8060 $\pm$ 0.1348	0.8316 $\pm$ 0.0003	0.2006 $\pm$ 0.0038	0.6000 $\pm$ 0.8000
Adapter		19.9880 $\pm$ 0.2398	0.8308 $\pm$ 0.0012	0.1895 $\pm$ 0.0052	0.0000 $\pm$ 0.0000
Distillaton		20.0620 $\pm$ 0.8880	<b>0.8361 <math>\pm</math> 0.0077</b>	0.1959 $\pm$ 0.0080	1.0000 $\pm$ 0.6325
REFINE		<b>21.7580 <math>\pm</math> 0.5958</b>	0.8308 $\pm$ 0.0072	<b>0.2139 <math>\pm</math> 0.0067</b>	<b>2.0000 <math>\pm</math> 1.0955</b>

Table 2: Single-source transfer with semantic confusion using CNN.

Dataset	Model	Accuracy	AUC	F1	Min CAcc
CIFAR-10	NoTrans	56.4400 $\pm$ 0.4787	0.9055 $\pm$ 0.0019	0.5599 $\pm$ 0.0051	32.8000 $\pm$ 4.5396
	LinearProb	53.1460 $\pm$ 1.0368	0.8883 $\pm$ 0.0145	0.5238 $\pm$ 0.0215	28.3600 $\pm$ 14.0419
	Adapter	51.6440 $\pm$ 0.9860	0.8960 $\pm$ 0.0022	0.5130 $\pm$ 0.0150	19.5200 $\pm$ 8.3180
	Distillation	54.8900 $\pm$ 0.4897	0.9063 $\pm$ 0.0013	0.5492 $\pm$ 0.0065	<b>41.9600 <math>\pm</math> 3.4256</b>
	REFINE	<b>56.5440 <math>\pm</math> 0.7302</b>	<b>0.9103 <math>\pm</math> 0.0012</b>	<b>0.5619 <math>\pm</math> 0.0103</b>	31.5800 $\pm$ 10.3147
CIFAR-100	NoTrans	17.5840 $\pm$ 0.2390	0.8271 $\pm$ 0.0033	0.1656 $\pm$ 0.0046	<b>1.0000 <math>\pm</math> 0.0000</b>
	LinearProb	22.4140 $\pm$ 0.4833	0.8687 $\pm$ 0.0011	0.2133 $\pm$ 0.0048	0.0000 $\pm$ 0.0000
	Adapter	22.6600 $\pm$ 0.2954	0.8676 $\pm$ 0.0014	0.2102 $\pm$ 0.0025	0.0000 $\pm$ 0.0000
	Distillation	19.5880 $\pm$ 0.6056	0.8659 $\pm$ 0.0034	0.1752 $\pm$ 0.0072	0.0000 $\pm$ 0.0000
	REFINE	<b>23.3080 <math>\pm</math> 0.4215</b>	<b>0.8719 <math>\pm</math> 0.0010</b>	<b>0.2264 <math>\pm</math> 0.0032</b>	0.4000 $\pm$ 0.4899

Table 3: Single-source transfer with imbalanced data using CNN.

differences in class number, semantics, and feature distributions. This includes CIFAR-10 $\rightarrow$ CIFAR-100 and CIFAR-100 $\rightarrow$ CIFAR-10, with 10,000 pretraining samples and 4,000 fine-tuning samples. We also evaluate the scenario of favorable transfer, where source and target domains are more closely aligned, including CIFAR-10 to STL-10 (Image), Clipart

Dataset	Model	Accuracy	AUC	F1	Min CAcc
CIFAR-100→10	NoTrans	<b>56.5820 ± 0.3659</b>	<b>0.9005 ± 0.0012</b>	<b>0.5634 ± 0.0046</b>	<b>37.2000 ± 3.4117</b>
	LinearProb	38.9260 ± 0.5463	0.8284 ± 0.0017	0.3815 ± 0.0051	16.9400 ± 3.7441
	Adapter	38.2320 ± 0.3111	0.8247 ± 0.0016	0.3754 ± 0.0071	16.4600 ± 5.4544
	REFINE	54.4000 ± 0.3336	0.8942 ± 0.0026	0.5406 ± 0.0051	33.6200 ± 2.8273
CIFAR-10→100	NoTrans	18.3200 ± 0.5254	0.8140 ± 0.0050	0.1774 ± 0.0052	1.0000 ± 0.8944
	LinearProb	7.0140 ± 0.3347	0.7489 ± 0.0011	0.0496 ± 0.0034	0.0000 ± 0.0000
	Adapter	6.5640 ± 0.2875	0.7499 ± 0.0008	0.0459 ± 0.0026	0.0000 ± 0.0000
	REFINE	<b>18.5880 ± 0.5494</b>	<b>0.8276 ± 0.0053</b>	<b>0.1787 ± 0.0057</b>	<b>1.4000 ± 0.8000</b>

Table 4: Single-source transfer under domain mismatches using CNN.

to Sketch (Image), USPS to MNIST (Image), Books to Kitchens (Text), and DVD to Electronics (Text). Here CIFAR-100→CIFAR-10 means that CIFAR-100 serves as the source and CIFAR-10 as the target. The distillation method is excluded in this comparison, as it assumes label correspondence for generating soft targets, which does not hold under domain shift. Again, REFINE clearly outperforms the baseline methods.

Table 4 reports the results for domain mismatches. With CIFAR-100 as the source domain for pretraining, Adapter and LinearProb suffer from severe negative transfer, with classification accuracy dropping by 20.35% and 19.66% relative to NoTrans. In contrast, REFINE only drops by 2.18%, which significantly mitigates negative transfer. With CIFAR-10 as the source domain, the trend is similar: Adapter and LinearProb degrade by 11.76% and 11.31%, whereas REFINE improves upon NoTrans across all metrics, indicating a successful knowledge transfer.

Table 5 reports the results for different application and data modalities. When the source and target domains are similar, effective transfer occurs, while REFINE still significantly outperforms all the baselines. For instance, for CIFAR-10→STL-10, REFINE outperforms Adapter by 4.13% in accuracy, by 0.0171 in AUC, by 0.0436 in F1 score, and by 10.30% in minimum class accuracy; and outperforms LinearProb by 3.15% in accuracy, by 0.0149 in AUC, by 0.0346 in F1 score, and by 7.05% in minimum class accuracy. It is also noted that REFINE is the only method achieving a nonzero minimum class accuracy over Sketch, and it reaches a minimum class accuracy of 31.62% over MNIST, whereas no other baselines exceed 10%. Furthermore, REFINE is the only method achieving positive transfer over text data Kitchens and Electronics, while both LinearProb and Adapter result in negative transfer.

#### 4.4 Multi-source transfer

Finally, we consider multi-source transfer. Thanks to its modular design, REFINE is naturally capable of handling multiple source domains and knowledge transfer while keeping inference overhead manageable. In contrast, multi-source transfer has been less explored in existing methods such as Adapters, LinearProbes and Distillation. For this experiment, we use CIFAR-10 with eight disjoint subsets of 2000 samples each as multiple sources. We train eight CNNs, and REFINE integrates the corresponding penultimate representations. We also compare with a naive method that trains on the concatenated external features. Both methods are matched in parameter count and training configuration, including dropout and epoch count (30). We evaluate three settings: the clean setting with clean labels and the usual learning rate of 0.01, the noisy setting with 50% label noise, and the low learning rate setting of 0.001 rate. REFINE clearly outperforms the baseline method, especially when the data is noisy or when the learning rate is low.

Dataset	Model	Accuracy	AUC	F1	Min CAcc
CIFAR10→STL	NoTrans	48.6925 ± 0.6338	0.8683 ± 0.0032	0.4831 ± 0.0089	<b>26.8000 ± 4.9006</b>
	LinearProb	50.2725 ± 0.3016	0.8795 ± 0.0015	0.4955 ± 0.0067	18.9250 ± 6.1546
	Adapter	49.2900 ± 0.7344	0.8773 ± 0.0008	0.4865 ± 0.0096	15.6750 ± 6.6340
	REFINE	<b>53.4175 ± 0.3628</b>	<b>0.8944 ± 0.0013</b>	<b>0.5301 ± 0.0053</b>	25.9750 ± 3.5693
Clipart→Sketch	NoTrans	18.8804 ± 1.3709	0.7170 ± 0.0117	0.1828 ± 0.0119	0.0000 ± 0.0000
	LinearProb	18.3430 ± 0.8649	0.7290 ± 0.0065	0.1727 ± 0.0087	0.0000 ± 0.0000
	Adapter	18.2356 ± 0.5807	<b>0.7369 ± 0.0059</b>	0.1549 ± 0.0040	0.0000 ± 0.0000
	REFINE	<b>20.3403 ± 0.4768</b>	0.7338 ± 0.0043	<b>0.1968 ± 0.0059</b>	<b>0.5263 ± 1.0526</b>
USPS→MNIST	NoTrans	62.0740 ± 8.7771	0.9566 ± 0.0073	0.5967 ± 0.0969	9.2863 ± 12.1512
	LinearProb	66.9960 ± 1.0095	0.9469 ± 0.0050	0.6563 ± 0.0086	9.1576 ± 3.5478
	Adapter	61.8660 ± 3.0334	0.9375 ± 0.0085	0.5952 ± 0.0441	8.8750 ± 7.2427
	REFINE	<b>70.0460 ± 2.1721</b>	<b>0.9582 ± 0.0053</b>	<b>0.6954 ± 0.0194</b>	<b>31.6157 ± 14.5527</b>
Books→Kitchen	NoTrans	71.6600 ± 1.3632	0.7848 ± 0.0155	0.7161 ± 0.0137	<b>68.6000 ± 2.9719</b>
	LinearProb	66.7400 ± 3.1455	0.7568 ± 0.0278	0.6571 ± 0.0401	51.5600 ± 9.7336
	Adapter	71.3400 ± 0.1356	0.7839 ± 0.0008	0.7111 ± 0.0015	62.8800 ± 2.9027
	REFINE	<b>72.7200 ± 1.6522</b>	<b>0.8147 ± 0.0133</b>	<b>0.7248 ± 0.0189</b>	65.5200 ± 6.4778
DVD→Electronics	NoTrans	68.5200 ± 2.8979	0.7585 ± 0.0304	0.6806 ± 0.0338	59.8000 ± 9.8298
	LinearProb	66.0600 ± 0.5122	0.7266 ± 0.0017	0.6580 ± 0.0072	58.3600 ± 4.5579
	Adapter	65.8600 ± 0.3200	0.7206 ± 0.0008	0.6577 ± 0.0037	61.4400 ± 2.5935
	REFINE	<b>70.3400 ± 0.9972</b>	<b>0.7886 ± 0.0115</b>	<b>0.6995 ± 0.0122</b>	<b>61.7200 ± 7.5181</b>

Table 5: Single-source transfer cross domain using CNN.

Figure 2 reports the results. For the clean setting, REFINE slightly outperforms Naive and stays well above NoTrans, implying its effective transfer capability. For the noisy data setting, REFINE significantly outperforms NoTrans as more external sources are used. Specifically, with all eight external sources, REFINE achieves the accuracy 52.5%, AUC 0.8962, and F1 0.5242, compared to Naive’s 48.2%, 0.8773, and 0.4744, and NoTrans’s 49.3%, 0.8803, and 0.4871. In this setting, Naive consistently underperforms NoTrans, implying negative transfer when external information is not integrated effectively. For the low learning rate setting, REFINE is beneficial compared to NoTrans when more external sources are integrated, while Naive suffers a dramatically degraded performance. With all eight external sources, REFINE achieves the accuracy 34.09%, outperforming NoTrans’s 30.16% and Naive’s 22.53%. The result under the low learning rate demonstrates that REFINE is easier and more efficient to train, and remains robust to a suboptimal training procedure.

## 5 Theoretical Analysis

In this section, we provide theoretical insights into why REFINE is effective in preventing negative transfer. Our main result shows that augmenting any fixed feature representation  $f_{\text{rep}}$  with a trainable residual connection  $h$  ensures that the learning rate of REFINE is never worse than that of a model trained from scratch using only the target data. Moreover, when  $f_{\text{rep}}$  captures a substantial part of the signal, the excess risk of REFINE interpolates smoothly between the classical non-parametric rate  $\tilde{O}(n^{-2\beta/(2\beta+d)})$  and a near-parametric rate  $\tilde{O}(p/n)$ , where  $d$  is the input dimension,  $\beta$  the Hölder smoothness of the residual and  $p$  the dimension of  $f_{\text{rep}}(x)$ .

We consider the non-parametric regression setup adopted in the statistical analysis of deep neural networks (Suzuki, 2018; Schmidt-Hieber, 2020; Kohler and Langer, 2021). Specifically, we observe  $n$  i.i.d. pairs  $(X_i, Y_i)_{i \in [n]} \subset [0, 1]^d \times \mathbb{R}$  following the regression

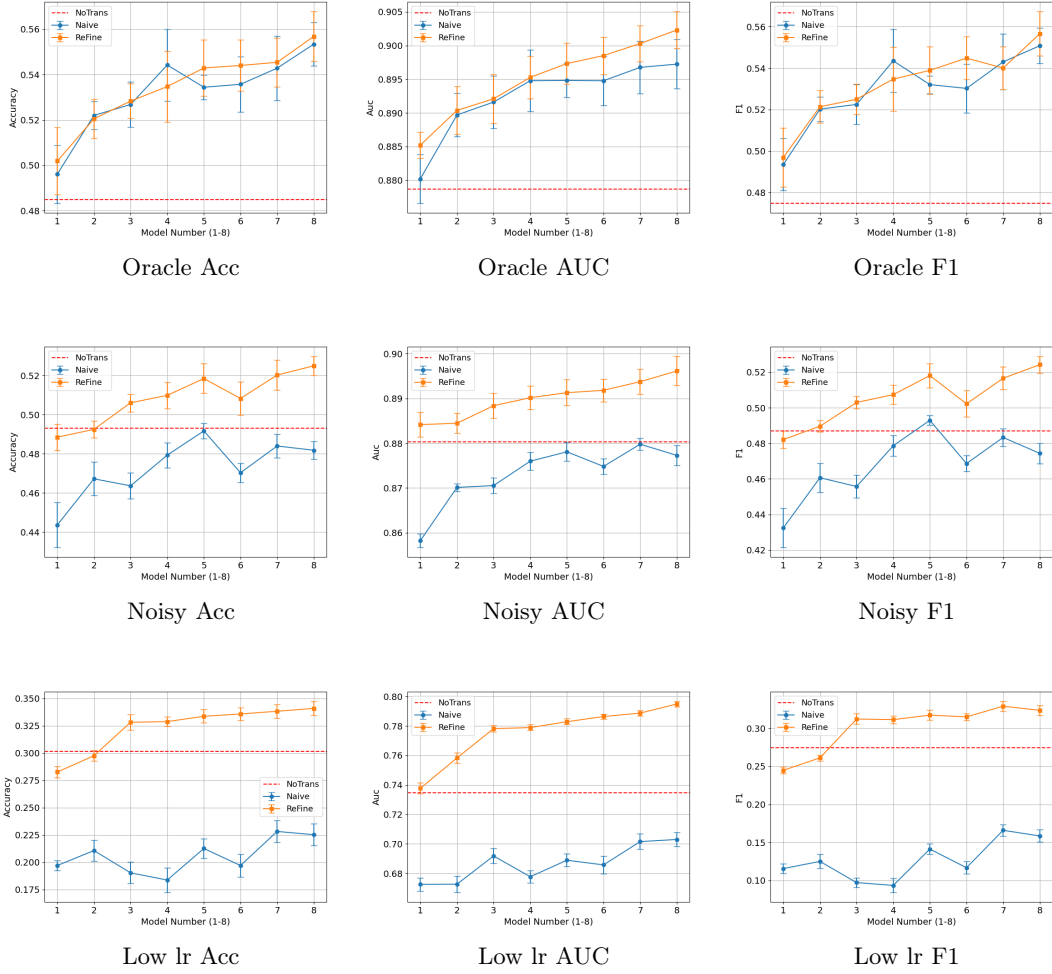


Figure 2: Multi-source transfer of REFINE.

model:

$$Y_i = f^*(X_i) + \epsilon_i,$$

where  $f^* : [0, 1]^d \rightarrow [-1, 1]$  is the ground-truth regression function, and the noise terms  $(\epsilon_i)_{i \in [n]}$  are assumed to be i.i.d. Gaussian, independent of  $(X_i)_{i \in [n]}$ .

**Hölder class functions** For a non-integer  $\beta > 0$ , the Hölder norm for functions that are  $\lfloor \beta \rfloor$ -times differentiable on  $[0, 1]^d$  is defined as

$$\|f\|_{\mathcal{C}^\beta} := \max \left\{ \max_{a \in \mathbb{N}^d: \|a\|_1 \leq \lfloor \beta \rfloor} \sup_{x \in [0, 1]^d} |\partial^a f(x)|, \max_{a \in \mathbb{N}^d: \|a\|_1 = \lfloor \beta \rfloor} \sup_{x \neq x' \in [0, 1]^d} \frac{|\partial^a f(x) - \partial^a f(x')|}{\|x - x'\|^{\beta - \lfloor \beta \rfloor}} \right\}.$$

Here,  $\partial^a$  denotes the partial derivative corresponding to the multi-index  $a$ . Accordingly, the unit ball in the Hölder space on  $[0, 1]^d$  is defined as

$$\mathcal{C}_u^\beta := \left\{ f : [0, 1]^d \rightarrow \mathbb{R} \mid f \text{ is } \lfloor \beta \rfloor\text{-times differentiable and } \|f\|_{\mathcal{C}^\beta} \leq 1 \right\}.$$

**ReLU Neural Networks for Residual Connection** We assume the residual function  $h(x)$  is a real-valued function. Fix width  $W \in \mathbb{N}_+$ , depth  $L \in \mathbb{N}_+$ , and parameter bound  $B > 0$ . We say  $h : \mathbb{R}^d \rightarrow \mathbb{R}$  is realized by a ReLU network of width at most  $W$ , depth at most  $L$ , and weight magnitude at most  $B$  if there exists  $L' \leq L$  and parameters  $A_\ell \in [-B, B]^{d_\ell \times d_{\ell-1}}$  and  $b_\ell \in [-B, B]^{d_\ell}$  for each layer  $\ell \in [L']$ , where  $d_0 := d$ ,  $d_{L'} = 1$ , and  $d_\ell \leq W$  for  $\ell \in [L' - 1]$ , such that

$$h(x) = A_{L'}x^{(L'-1)} + b_{L'}, \text{ with } x^{(\ell)} = \sigma(A_\ell x^{(\ell-1)} + b_\ell) \text{ for } \ell \in [L' - 1] \text{ and } x^{(0)} = x, \quad (2)$$

where  $\sigma(z) = \max\{0, z\}$  is the ReLU activation function applied element-wise. The class of all functions defined by equation 2 is denoted by  $\mathcal{H}_d(W, L, B)$ . To facilitate convergence analysis, we also introduce the clipped neural network class  $\bar{\mathcal{H}}_d(W, L, B) := \{x \mapsto \min\{1, \max\{-1, h(x)\}\} \mid h \in \mathcal{H}_d(W, L, B)\}$ , which restricts the network output to the interval  $[-1, 1]$ .

**Empirical Risk Minimization for REFINe** While REFINe is trained under cross-entropy loss, for tractability of analysis we focus on the squared loss  $\ell(y, y') = (y - y')^2$  as in several recent theoretical studies (Han et al., 2021; Zhou et al., 2022). Let  $f_{\text{rep}} : [0, 1]^d \rightarrow \mathcal{B}_p(1)$  denote a given external representation, where  $\mathcal{B}_p(R) = \{u \in \mathbb{R}^p : \|u\|_2 \leq R\}$  is a ball in  $\mathbb{R}^p$  with radius  $R$  centered at 0.

Define the REFINe function class with a linear adapter  $w(f_{\text{rep}}(x), h(x)) = v^\top f_{\text{rep}}(x) + uh(x)$  as

$$\mathcal{G}_{d,p}(W, L, B; f_{\text{rep}}) = \left\{ g : [0, 1]^d \rightarrow \mathbb{R} \mid \begin{array}{l} g(x) = v^\top f_{\text{rep}}(x) + uh(x), \\ |u| \leq 1, \|v\| \leq 1, h \in \bar{\mathcal{H}}_d(W, L, B) \end{array} \right\}.$$

We train  $\hat{g}$  via empirical risk minimization using parameters  $W, L, B$  and  $f_{\text{rep}}$ :

$$\hat{g} = \arg \min_{g \in \mathcal{G}_{d,p}(W, L, B; f_{\text{rep}})} \frac{1}{n} \sum_{i \in [n]} \ell(g(X_i), Y_i). \quad (3)$$

Our goal is to derive a bound on the generalization error of  $\hat{g}$ . For simplicity, assume the marginal distribution  $\mathbb{P}_X$  admits a density on  $[0, 1]^d$  bounded by an absolute constant. The following theorem establishes a bound on the prediction risk of REFINe.

**Theorem 5.1.** *Fix any external representation  $f_{\text{rep}} : [0, 1]^d \rightarrow \mathcal{B}_p(1)$  and define the best linear probe*

$$v^* = \arg \min_{v \in \mathbb{R}^p} \mathbb{E}[\{v^\top f_{\text{rep}}(X_1) - f^*(X_1)\}^2].$$

Assume  $\|v^*\| \leq 1$  and that the residual  $f^* - v^{*\top} f_{\text{rep}}$  lies in the unit Hölder ball  $\mathcal{C}_u^\beta$  with a non-integer  $\beta > 0$ . Let  $\rho > 0$  be a tuning parameter (which serves as a proxy for the residual norm), and choose network parameters

$$L = c_1, \quad W = c_2 \max\{n^{d/(2\beta+d)} \rho^{2d/(2\beta+d)}, 1\}, \quad B = \max\{n\rho^2, 1\}^{c_3}, \quad (4)$$

where  $c_1, c_2, c_3 > 0$  depend on  $\beta$  and  $d$ . Let  $\hat{g}$  be the empirical risk minimizer in equation 3 with the parameter choice in equation 4. Then, there exists a constant  $C > 0$  depending on  $\beta$  and  $d$  such that

$$\mathbb{E}[\|\hat{g} - f^*\|_{L_2}^2] \leq C \left\{ \left( \rho^{2d/(2\beta+d)} \log n + \rho^{*2} \rho^{-4\beta/(2\beta+d)} \right) n^{-2\beta/(2\beta+d)} + \frac{p \log n}{n} \right\},$$

where  $\rho^* := \|v^{*\top} f_{\text{rep}} - f^*\|_{\mathcal{C}^\beta}$ .

Theorem 5.1 states that the prediction risk bound is decomposed into (1) a parametric error term  $p \log n/n$  from estimating  $v^*$ , and (2) a nonparametric term  $n^{-2\beta/(2\beta+d)}$  weighted by  $\tilde{O}(\rho^{2d/(2\beta+d)} + \rho^{*2} \rho^{-4\beta/(2\beta+d)})$  from estimating the residual. Importantly, choosing  $\rho = \rho^*$  balances the weight and yields the oracle rate

$$\tilde{O}(\rho^{*2d/(2\beta+d)} n^{-2\beta/(2\beta+d)} + p/n).$$

Here,  $\rho$  is a tuning parameter that can be selected via cross-validation in practice. Furthermore, training procedures such as SGD can introduce implicit regularization, for example, through early stopping which effectively limits the complexity of the network.

*Proof Sketch of Theorem 5.1.* When an auxiliary representation  $f_{\text{rep}} : [0, 1]^d \rightarrow \mathbb{R}^p$  is available, we can decompose  $f^*$  as:

$$f^*(x) = \underbrace{f^*(x) - v^\top f_{\text{rep}}(x)}_{\text{residual component}} + \underbrace{v^\top f_{\text{rep}}(x)}_{\text{linear in } f_{\text{rep}}(x)} \quad \text{for any fixed } v \in \mathbb{R}^p.$$

If  $f_{\text{rep}}$  is a strong predictor, meaning there exists a linear transformation  $x \mapsto v^\top f_{\text{rep}}(x)$  that closely approximates  $f^*$ , the learning task reduces to estimating the smaller residual function  $f^*(x) - v^\top f_{\text{rep}}(x)$  and the simple component  $x \mapsto v^\top f_{\text{rep}}(x)$ .

Recall that REFINe learns a function of the form  $g(x) = uh(x) + v^\top f_{\text{rep}}(x)$ . Here,  $h(x)$  captures the residual component, while  $v^\top f_{\text{rep}}(x)$  represents the component based on the external representation. When  $f_{\text{rep}}$  is informative, the residual becomes simpler, so one can use a lower-complexity network for  $h(x)$ , reducing the overall sample complexity.  $\square$

The formal proof of Theorem 5.1 is deferred to the Appendix A.

*Remark 5.2.* Suppose in addition that  $f^*$  is in the Hölder ball  $\mathcal{C}_u^\beta$ . When the external representation is highly informative in the sense that the residual norm  $\rho^* = \|v^{*\top} f_{\text{rep}} - f^*\|_{\mathcal{C}^\beta}$  is small, and the learning task reduces to approximating a simpler residual. Consequently, this allows the use of a smaller network class and achieving  $\tilde{O}(\rho^{*2d/(2\beta+d)} n^{-2\beta/(2\beta+d)} + p/n)$  under the oracle choice of radius  $\rho$ . In this regime, useful knowledge is indeed transferred from the source to the target domain, yielding tangible benefits. Conversely, when the external representation does not align well with the target distribution,  $\rho^*$  will be of constant order. In this case, the nonparametric term dominates the bound, resulting in the prediction risk scaling as  $\tilde{O}(n^{-2\beta/(2\beta+d)})$ , nearly matching the minimax optimal rate for  $\beta$ -Hölder regression function (Tsybakov, 2008) when we train  $g_{\text{sc}}$  using only the target data  $(Y_i)_{i \in [n]}$  on  $(X_i)_{i \in [n]}$ . Hence, REFINe prevents the negative transfer, and will never underperform the standard nonparametric methods in terms of the rate of convergence.

*Remark 5.3.* In the linear probing approach, one fits a linear map  $w_{\text{ft}}(x) = v^\top x$  on top of frozen  $f_{\text{rep}}$ . If there exists  $v^* \in \mathbb{R}^p$  such that  $v^* \circ f_{\text{rep}} = f^*$  on the target distribution, then estimating the  $p$  coefficients of  $v^*$  attains the parametric rate  $O(p/n)$ . However, under distribution shift the equality  $v^{*\top} f_{\text{rep}} = f^*$  may not hold, leaving an irreducible bias  $\min_{v \in \mathbb{R}^p} \|f^* - v^\top f_{\text{rep}}\|_{L_2}$ . The same intuition holds for nonlinear adapters: if the frozen features  $f_{\text{rep}}$  have “lost” information about  $x$ , no choice of adapter can recover it. In contrast, REFINe learns a residual function  $h(x)$  over the raw input space, which is more flexible and can adapt to the true residual function. This is a key advantage of REFINe over the linear probing.

## 6 Conclusion

We present REFINe, a simple yet effective approach for safe transfer learning. By combining frozen pretrained features with a trainable encoder of raw features, REFINe guarantees performance no worse than training from scratch and adapts to external representations. Our theoretical analysis provides formal guarantees on the prediction risk, and extensive numerical experiments across diverse settings show consistent improvements over the baselines. These results demonstrate REFINe as a practical and robust transfer learning approach.

REFINE can be extended to a wider range of tasks and architectures. Its residual integration strategy may also inspire a new class of robust adapters that scale effectively to larger models such as LLMs. We observe that REFINe achieves a strong generalization and subgroup performance, particularly in least represented classes, motivating further research into its out-of-distribution behavior and theoretical guarantees on subgroup risk. While we currently use the penultimate layer of the pretrained model, future work may explore sparse integration across all layers, such as lasso-based selection, to further improve the performance. Given its natural design for multi-source integration, it would also be interesting to apply influence functions or gradient-based analyses to interpret which sources contribute most. We leave these as future directions.

## Acknowledgement

We are grateful to Shuoxun Xu for the helpful discussion during this project. The research of LZ is partially supported by NSF CAREER DMS-2340241. The research of LL is partially supported by NSF grant CIF-2102227, and NIH grants R01AG062542 and R01AG080043.

## References

- Anaby-Tavor, A., Carmeli, B., Goldbraich, E., Kantor, A., Kour, G., Shlomov, S., Tepper, N., and Zwerdling, N. (2019). Do not have enough data? deep learning to the rescue! In *AAAI Conference on Artificial Intelligence*.
- Blitzer, J., Dredze, M., and Pereira, F. (2007). Biographies, Bollywood, boom-boxes and blenders: Domain adaptation for sentiment classification. In Zaenen, A. and van den Bosch, A., editors, *Proceedings of the 45th Annual Meeting of the Association of Computational Linguistics*, pages 440–447, Prague, Czech Republic. Association for Computational Linguistics.
- Bowles, C., Chen, L., Guerrero, R., Bentley, P., Gunn, R., Hammers, A., Dickie, D. A., Hernández, M. V., Wardlaw, J., and Rueckert, D. (2018). Gan augmentation: Augmenting training data using generative adversarial networks.
- Cheng Ju, A. B. and van der Laan, M. (2018). The relative performance of ensemble methods with deep convolutional neural networks for image classification. *Journal of Applied Statistics*, 45(15):2800–2818. PMID: 31631918.
- Coates, A., Ng, A., and Lee, H. (2011). An analysis of single-layer networks in unsupervised feature learning. In Gordon, G., Dunson, D., and Dudík, M., editors, *Proceedings of the Fourteenth International Conference on Artificial Intelligence and Statistics*, volume 15 of *Proceedings of Machine Learning Research*, pages 215–223, Fort Lauderdale, FL, USA. PMLR.

- Compton, R., Zhang, L., Puli, A., and Ranganath, R. (2023). When more is less: Incorporating additional datasets can hurt performance by introducing spurious correlations.
- Ghorbani, A. and Zou, J. (2019). Data shapley: Equitable valuation of data for machine learning.
- Gou, J., Yu, B., Maybank, S. J., and Tao, D. (2021). Knowledge distillation: A survey. *International Journal of Computer Vision*, 129(6):1789–1819.
- Gretton, A., Borgwardt, K. M., Rasch, M. J., Schölkopf, B., and Smola, A. (2012). A kernel two-sample test. *J. Mach. Learn. Res.*, 13(null):723–773.
- Grover, P., Chaturvedi, K., Zi, X., Saxena, A., Prakash, S., Jan, T., and Prasad, M. (2023). Ensemble transfer learning for distinguishing cognitively normal and mild cognitive impairment patients using mri. *Algorithms*, 16(8).
- Han, X., Pappayan, V., and Donoho, D. L. (2021). Neural collapse under mse loss: Proximity to and dynamics on the central path. *arXiv preprint arXiv:2106.02073*.
- He, K., Zhang, X., Ren, S., and Sun, J. (2016). Deep residual learning for image recognition. In *Proceedings of the IEEE conference on computer vision and pattern recognition*, pages 770–778.
- Hinton, G., Vinyals, O., and Dean, J. (2015). Distilling the knowledge in a neural network.
- Hosna, A., Merry, E., Gyalmo, J., Alom, Z., Aung, Z., and Azim, M. A. (2022). Transfer learning: a friendly introduction. *Journal of Big Data*, 9(1):102. Epub 2022 Oct 22.
- Houlsby, N., Giurgiu, A., Jastrzebski, S., Morrone, B., de Laroussilhe, Q., Gesmundo, A., Attariyan, M., and Gelly, S. (2019). Parameter-efficient transfer learning for nlp.
- Jain, A., Montanari, A., and Sasoglu, E. (2024). Scaling laws for learning with real and surrogate data.
- Jha, R., Lovering, C., and Pavlick, E. (2020). Does data augmentation improve generalization in nlp?
- Ke, G., Meng, Q., Finley, T., Wang, T., Chen, W., Ma, W., Ye, Q., and Liu, T.-Y. (2017). Lightgbm: A highly efficient gradient boosting decision tree. In Guyon, I., Luxburg, U. V., Bengio, S., Wallach, H., Fergus, R., Vishwanathan, S., and Garnett, R., editors, *Advances in Neural Information Processing Systems*, volume 30. Curran Associates, Inc.
- Kohler, M. and Langer, S. (2021). On the rate of convergence of fully connected deep neural network regression estimates. *The Annals of Statistics*, 49(4):2231–2249.
- Krizhevsky, A. (2009). Learning multiple layers of features from tiny images. Technical report, University of Toronto. Technical Report.
- Kumar, A., Raghunathan, A., Jones, R., Ma, T., and Liang, P. (2022). Fine-tuning can distort pretrained features and underperform out-of-distribution.
- Li, Y.-F., Guo, L.-Z., and Zhou, Z.-H. (2021). Towards safe weakly supervised learning. *IEEE Transactions on Pattern Analysis and Machine Intelligence*, 43(1):334–346.

- Lin, C.-H., Kaushik, C., Dyer, E. L., and Muthukumar, V. (2022). The good, the bad and the ugly sides of data augmentation: An implicit spectral regularization perspective. *J. Mach. Learn. Res.*, 25:91:1–91:85.
- Lin, Y. P. and Jung, T. P. (2017). Improving eeg-based emotion classification using conditional transfer learning. *Frontiers in Human Neuroscience*, 11:334. Published on June 27, 2017.
- Mohammed, A. and Kora, R. (2023). A comprehensive review on ensemble deep learning: Opportunities and challenges. *Journal of King Saud University - Computer and Information Sciences*, 35(2):757–774.
- Nakada, R. and Imaizumi, M. (2020). Adaptive approximation and generalization of deep neural network with intrinsic dimensionality. *Journal of Machine Learning Research*, 21(174):1–38.
- Nguyen, T., Ilharco, G., Wortsman, M., Oh, S., and Schmidt, L. (2023). Quality not quantity: On the interaction between dataset design and robustness of clip.
- Peng, X., Bai, Q., Xia, X., Huang, Z., Saenko, K., and Wang, B. (2019). Moment matching for multi-source domain adaptation. In *Proceedings of the IEEE International Conference on Computer Vision*, pages 1406–1415.
- Petersen, P. and Voigtlaender, F. (2018). Optimal approximation of piecewise smooth functions using deep relu neural networks. *Neural Networks*, 108:296–330.
- Schmidt-Hieber, J. (2020). Nonparametric regression using deep neural networks with relu activation function. *The Annals of Statistics*.
- Smyl, S. and Kuber, K. (2016). Data preprocessing and augmentation for multiple short time series forecasting with recurrent neural networks. In *Proceedings of the 36th International Symposium on Forecasting*, pages 1–6, Santander, Spain.
- Suzuki, T. (2018). Adaptivity of deep relu network for learning in besov and mixed smooth besov spaces: optimal rate and curse of dimensionality. *arXiv preprint arXiv:1810.08033*.
- Tsybakov, A. (2008). *Introduction to Nonparametric Estimation*. Springer Series in Statistics. Springer New York.
- Zhang, W., Deng, L., Zhang, L., and Wu, D. (2023). A survey on negative transfer. *IEEE/CAA Journal of Automatica Sinica*, 10(2):305–329.
- Zhou, J., Li, X., Ding, T., You, C., Qu, Q., and Zhu, Z. (2022). On the optimization landscape of neural collapse under mse loss: Global optimality with unconstrained features. In *International Conference on Machine Learning*, pages 27179–27202. PMLR.

## A Proofs of Main Results

In this section, we prove the main results from Section 5.

**Additional Notation** Let  $\|\cdot\|_{L_q}$  denote the  $L_q$  norm under the probability measure  $\mathbb{P}_X$  for any  $q \in [1, \infty]$ , where  $\mathbb{P}_X$  is the distribution of  $X_i$  in the training data. For  $a, b \in \mathbb{R}$ , we define  $a \wedge b = \min\{a, b\}$  and  $a \vee b = \max\{a, b\}$ .

We now prove the proof of the main theorem on the prediction risk of REFINe.

*Proof of Theorem 5.1.* Recall that  $v^*$  is the optimal linear probe of  $f_{\text{rep}}$ , i.e.,

$$v^* = \arg \min_{v \in \mathbb{R}^p} \mathbb{E}[\{f^*(X) - v^\top f_{\text{rep}}(X)\}^2].$$

We begin by observing that the difficulty of the estimation problem is governed by the residual  $r^* := f^* - v^{*\top} f_{\text{rep}}$ , since  $f_{\text{rep}}$  is assumed to be known, and  $v^{*\top} f_{\text{rep}}$  can be seen as a linear function of the known quantity. By appropriately choosing the parameters  $W$ ,  $L$ , and  $B$ , we control the complexity of the neural network, and the bias of estimating  $r^*$ .

Specifically, choose

$$L = (2 + \lceil \log_2 \beta \rceil) \left( 11 + \frac{\beta}{d} \right), \quad W = c'_1 \epsilon^{-d/\beta}, \quad B = \epsilon^{-c'_2}, \quad (5)$$

where  $c'_1, c'_2 > 0$  are constants appearing in Lemma B.2. Define  $\rho^* := \|r^*\|_{\mathcal{C}^\beta}$ . Set

$$\epsilon := n^{-\beta/(2\beta+d)} \rho^{-2\beta/(2\beta+d)} \wedge 1, \quad (6)$$

where  $\rho > 0$  is some tuning parameter.

Note that  $\sup_{g \in \mathcal{G}_{d,p}(W, L, B; f_{\text{rep}})} \|g\|_{L_\infty} \leq 2$ . From Lemma B.3 with the choice  $\delta \leftarrow 1/n$ , we have

$$\mathbb{E}[\|\hat{g} - f^*\|_{L_2}^2] \lesssim \left( \inf_{g \in \mathcal{G}} \|g - f^*\|_{L_2}^2 + \frac{\log \mathcal{N}(1/n, \mathcal{G}_{d,p}(W, L, B; f_{\text{rep}}), \|\cdot\|_{L_\infty})}{n} + \frac{1}{n} \right).$$

Next we compute the first term and the second term separately.

**Part 1: Bounding the first term.** Notice that  $\rho^* \leq 1$  by assumption  $r^* = f^* - v^{*\top} f_{\text{rep}} \in \mathcal{C}_u^\beta$ . Rescale the residual by noting that  $(1/\rho^*)r^* \in \mathcal{C}_u^\beta$ . Then, by Lemma B.2, there exists a neural network  $r_{\text{NN}} \in \mathcal{H}_d(W, L, B)$  such that

$$\|r_{\text{NN}} - (1/\rho^*)r^*\|_{L_2} \lesssim \epsilon. \quad (7)$$

This inequality provides the approximation error of the ReLU network class. To translate this result to the bias term  $\|g - f^*\|_{L_2}^2$ , we proceed as follows. Write

$$r_{\text{NN}} = r_{\text{NN},L} \circ r_{\text{NN},L-1} \circ \cdots \circ r_{\text{NN},1}(x),$$

where  $r_{\text{NN},\ell}(x) = \sigma(A_\ell x + b_\ell)$  for  $\ell \in [L-1]$  and  $r_{\text{NN},L}(x) = A_L x + b_L$ . Define  $r'_{\text{NN},L}(x) = (\rho^* A'_L)x + (\rho^* b'_L)$  to approximate  $\rho^* r_{\text{NN}}$ . Then, it follows that the function

$$g^\circ(x) := 1 \wedge ((-1) \vee r'_{\text{NN},L} \circ r_{\text{NN},L-1} \circ \cdots \circ r_{\text{NN},1}(x)) + v^{*\top} f_{\text{rep}}(x)$$

belongs to  $\mathcal{G}_{d,p}(W, L, B; f_{\text{rep}})$  since  $\rho^* \leq 1$  and  $\|v^*\| \leq 1$ . Moreover, we can write  $g^\circ$  as

$$g^\circ(x) = 1 \wedge ((-1) \vee \rho^* r_{\text{NN}}(x)) + v^{*\top} f_{\text{rep}}(x).$$

Using equation 7, we have

$$\begin{aligned}
\mathbb{E}[\{g^\circ(X_1) - f^*(X_1)\}^2]^{1/2} &= \|1 \wedge ((-1) \vee \rho^* r_{\text{NN}}) + v^{*\top} f_{\text{rep}} - f^*\|_{L_2} \\
&= \rho^* \left\| \frac{1}{\rho^*} \wedge \left( -\frac{1}{\rho^*} \vee r_{\text{NN}} \right) - \frac{1}{\rho^*} r^* \right\|_{L_2} \\
&\leq \rho^* \left\| r_{\text{NN}} - \frac{1}{\rho^*} r^* \right\|_{L_2} \\
&\lesssim \rho^* \epsilon,
\end{aligned}$$

where we used the fact that  $\|r^*/\rho^*\|_{L_\infty} \leq \|r^*/\rho^*\|_{C^\beta} \leq 1/\rho^*$ . Thus,

$$\inf_{g \in \mathcal{G}_{d,p}(W,L,B;f_{\text{rep}})} \mathbb{E}[\|g - f^*\|_{L_2}^2] \leq \mathbb{E}[\|g^\circ - f^*\|_{L_2}^2] \lesssim \rho^{*2} \epsilon^2.$$

**Part 2: Bounding the second term.** The covering number bound from Lemma B.4 with the choice of  $W, L, B$  in equation 5, we have

$$\frac{\log \mathcal{N}(1/n, \mathcal{G}_{d,p}(W, L, B; f_{\text{rep}}), \|\cdot\|_{L_\infty})}{n} \leq \frac{C'}{n} (\epsilon^{-d/\beta} + p) \log \left( \frac{n}{\epsilon} \right),$$

where  $C'$  is a constant depending on  $d$  and  $\beta$ .

**Part 3: Balancing terms.** Finally, we combine the results from part 1 and part 2. Recalling the choice of  $\epsilon$  in equation 6, we consider two cases depending on the value of  $\rho$ .

When  $1/\sqrt{n} \leq \rho$ , we have  $\epsilon = (n\rho^2)^{-\beta/(2\beta+d)}$ . In this case, the bound becomes

$$\begin{aligned}
\mathbb{E}[\|\hat{g} - f^*\|_{L_2}^2] &\leq \rho^{*2} \rho^{-4\beta/(2\beta+d)} n^{-2\beta/(2\beta+d)} + C' \left( \rho^{2d/(2\beta+d)} n^{-2\beta/(2\beta+d)} + \frac{p}{n} \right) \log n \\
&\leq (C' + 1) \left( (\rho^{*2} \rho^{-4\beta/(2\beta+d)} + \rho^{2d/(2\beta+d)} \log n) n^{-2\beta/(2\beta+d)} + \frac{p \log n}{n} \right). \quad (8)
\end{aligned}$$

When  $\rho \leq 1/\sqrt{n}$  (so that  $\epsilon = 1$ ), the bound becomes

$$\mathbb{E}[\|\hat{g} - f^*\|_{L_2}^2] \leq \rho^{*2} + C' \frac{p \log n}{n} \leq (C' + 1) \left( \rho^{*2} \rho^{-4\beta/(2\beta+d)} n^{-2\beta/(2\beta+d)} + \frac{p \log n}{n} \right). \quad (9)$$

Combining the bounds in equation 8 and equation 9, we obtain the desired result.  $\square$

## B Auxiliary Results

We borrow the following entropy bound for  $\mathcal{H}_d(W, L, B)$ .

**Lemma B.1** (Lemma 21 from Nakada and Imaizumi (2020)). *Fix any  $W, L$ , and  $B > 0$ . Then, we have the covering number bound*

$$\log \mathcal{N}(\epsilon, \mathcal{H}_d(W, L, B), \|\cdot\|_{L_\infty}) \leq W \log \left( \frac{2LB^L(W+1)^L}{\epsilon} \right).$$

We also utilize the following approximation result from Petersen and Voigtlaender (2018), adapted to consider  $L_2$  approximation error with respect to the probability measure  $\mathbb{P}_X$  over the domain  $[0, 1]^d$ , rather than the original  $L_2$  error with a uniform measure on  $[-1/2, 1/2]^d$ .

**Lemma B.2** (Modification of Theorem 3.1 from Petersen and Voigtlaender (2018)). *Fix  $d \in \mathbb{N}_+$  and  $\beta > 0$ . Suppose that  $\mathbb{P}_X$  has a density bounded by  $O(1)$ . Then, there exist constants  $c'_1, c'_2 > 0$ , depending on  $d$  and  $\beta$ , such that for any  $\epsilon \in (0, 1/2)$ , if one chooses  $W, L$ , and  $B$  satisfying*

$$L \leq (2 + \lceil \log_2 \beta \rceil) \left( 11 + \frac{\beta}{d} \right), \quad W \leq c'_1 \epsilon^{-d/\beta}, \quad B \leq \epsilon^{-c'_2},$$

then

$$\sup_{f^\# \in \mathcal{C}_u^\beta} \inf_{f_{NN} \in \mathcal{H}_d(W, L, B)} \|f_{NN} - f^\#\|_{L_2} \lesssim \epsilon.$$

We also need the following lemma, which provides a bound on the prediction risk of the empirical risk minimizer in terms of the covering number of the function class and the approximation error.

**Lemma B.3** (Modification to Lemma 4 from Schmidt-Hieber (2020)). *Let  $\mathcal{G}$  be a function class, and let  $\hat{g}$  be the minimizer of the empirical risk  $(1/n) \sum_{i \in [n]} \ell(\hat{g}(X_i), Y_i)$  over  $\mathcal{G}$  under the data generating process introduced in Section 5. Assume that  $\{f^*\} \cup \mathcal{G} \subset \{[0, 1]^d \rightarrow [-F, F]\}$  for some  $F \geq 1$ . Then there exists a universal constant  $C_0 > 0$  such that*

$$\mathbb{E}[\|\hat{g} - f^*\|_{L_2}^2] \leq C_0 \left( \inf_{g \in \mathcal{G}} \|g - f^*\|_{L_2}^2 + F^2 \frac{\log \mathcal{N}(\delta, \mathcal{G}, \|\cdot\|_{L_\infty})}{n} + \delta F \right).$$

The following lemma provides a bound on the covering number of the REFINe class  $\mathcal{G}_{d,p}(W, L, B; f_{\text{rep}})$ .

**Lemma B.4.** *Fix  $W \in \mathbb{N}_+$ ,  $L \in \mathbb{N}_+$ ,  $B > 0$ , and  $\delta > 0$ . Then, there exists a universal constant  $C > 0$  such that*

$$\log \mathcal{N}(\delta, \mathcal{G}_{d,p}(W, L, B; f_{\text{rep}}), \|\cdot\|_{L_\infty}) \leq C \left\{ W \log \left( \frac{LB^L(W+1)^L}{\delta} \right) + p \log \left( \frac{1}{\delta} \right) \right\}.$$

*Proof of Lemma B.4.* We next bound the covering number  $\mathcal{N}(\delta, \mathcal{G}_{d,p}(W, L, B; f_{\text{rep}}), \|\cdot\|_{L_\infty})$ . Note that for any  $\delta > 0$ , we have

$$\begin{aligned} & \log \mathcal{N}(\delta, \mathcal{G}_{d,p}(W, L, B; f_{\text{rep}}), \|\cdot\|_{L_\infty}) \\ & \leq \log \mathcal{N} \left( \frac{\delta}{2}, \{x \mapsto uh(x) \mid u \in [-1, 1], h \in \bar{\mathcal{H}}_d(W, L, B)\}, \|\cdot\|_{L_\infty} \right) \\ & \quad + \log \mathcal{N} \left( \frac{\delta}{2}, \{x \mapsto v^\top f_{\text{rep}}(x) \mid v \in \mathcal{B}_p(1)\}, \|\cdot\|_{L_\infty} \right). \end{aligned} \quad (10)$$

Recall that  $f_{\text{rep}} : [0, 1]^d \rightarrow \mathcal{B}_p(1)$ . Since  $\|v^\top f_{\text{rep}} - v'^\top f_{\text{rep}}\|_{L_\infty} \leq \|v - v'\|_2$  for any  $v, v' \in \mathcal{B}_p(1)$ , a standard argument shows that

$$\mathcal{N} \left( \frac{\delta}{2}, \{x \mapsto v^\top f_{\text{rep}}(x) \mid v \in \mathcal{B}_p(1)\}, \|\cdot\|_{L_\infty} \right) \leq \mathcal{N} \left( \frac{\delta}{2}, \mathcal{B}_p(1), \|\cdot\|_2 \right) \leq \left( \frac{6}{\delta} \right)^p. \quad (11)$$

Furthermore, since  $\|u_1 h_1 - u_2 h_2\|_{L_\infty} \leq \|h_1 - h_2\|_{L_\infty} + |u_1 - u_2|$  for any  $u_1, u_2 \in [-1, 1]$  and  $h_1, h_2 \in \bar{\mathcal{H}}_d(W, L, B)$ , we have

$$\begin{aligned} & \mathcal{N} \left( \frac{\delta}{2}, \{x \mapsto uh(x) \mid u \in [-1, 1], h \in \bar{\mathcal{H}}_d(W, L, B)\}, \|\cdot\|_{L_\infty} \right) \\ & \leq \mathcal{N} \left( \frac{\delta}{4}, [-1, 1], |\cdot| \right) \mathcal{N} \left( \frac{\delta}{4}, \bar{\mathcal{H}}_d(W, L, B), \|\cdot\|_{L_\infty} \right) \\ & \lesssim \frac{1}{\delta} \mathcal{N} \left( \frac{\delta}{4}, \mathcal{H}_d(W, L, B), \|\cdot\|_{L_\infty} \right). \end{aligned} \quad (12)$$

Dataset	Model	Accuracy	AUC	F1	Min CAcc
CIFAR-10	NoTrans	56.0500 ± 0.5350	0.9035 ± 0.0023	0.5588 ± 0.0059	34.0400 ± 5.0254
	LinearProb	65.4520 ± 0.3708	0.9367 ± 0.0005	0.6541 ± 0.0035	44.5400 ± 6.5722
	Adapter	65.1600 ± 0.1638	0.9354 ± 0.0006	0.6525 ± 0.0008	<b>46.3400 ± 1.2627</b>
	Distillation	59.6220 ± 0.3083	0.9180 ± 0.0014	0.5956 ± 0.0034	40.9400 ± 3.1059
	REFINE	<b>65.5720 ± 0.0773</b>	<b>0.9379 ± 0.0009</b>	<b>0.6559 ± 0.0015</b>	44.5200 ± 4.5411
CIFAR-100	NoTrans	17.6560 ± 0.7171	0.8208 ± 0.0045	0.1676 ± 0.0067	0.6000 ± 0.4899
	LinearProb	<b>26.2640 ± 0.6029</b>	<b>0.8838 ± 0.0013</b>	0.2542 ± 0.0073	1.2000 ± 1.1662
	Adapter	26.2320 ± 0.4569	0.8836 ± 0.0028	0.2506 ± 0.0073	<b>2.0000 ± 1.0954</b>
	Distillation	22.9340 ± 0.7675	0.8779 ± 0.0054	0.2228 ± 0.0083	<b>2.0000 ± 0.8944</b>
	REFINE	26.1880 ± 0.4939	0.8824 ± 0.0021	<b>0.2563 ± 0.0056</b>	1.8000 ± 0.9798

Table 6: Single-source transfer with clean data using CNN.

Dataset	Model	Accuracy	AUC	F1	Min CAcc
CIFAR-10	NoTrans	44.93 ± 0.586	0.86564 ± 0.00371	0.44552 ± 0.00806	18.98 ± 7.493
	LinearProb	<b>59.458 ± 0.175</b>	<b>0.919485 ± 0.001052</b>	<b>0.592373 ± 0.000889</b>	39.88 ± 1.677
	Adapter	58.462 ± 0.436	0.914027 ± 0.001007	0.579931 ± 0.005536	36.88 ± 4.423
	Distillation	47.048 ± 1.124	0.876883 ± 0.003927	0.472139 ± 0.011201	25.62 ± 3.846
	REFINE	58.306 ± 0.396	0.914195 ± 0.000766	0.582305 ± 0.003543	<b>40.26 ± 2.546</b>
CIFAR-100	NoTrans	15.318 ± 0.333	0.84489 ± 0.00210	0.13584 ± 0.00411	0.000 ± 0.000
	LinearProb	<b>26.126 ± 0.196</b>	<b>0.88847 ± 0.00085</b>	<b>0.25748 ± 0.00222</b>	<b>4.000 ± 1.789</b>
	Adapter	24.850 ± 0.479	0.88462 ± 0.00259	0.23662 ± 0.00599	1.200 ± 0.748
	Distillation	18.932 ± 0.198	0.87613 ± 0.00121	0.17474 ± 0.00440	0.400 ± 0.490
	REFINE	25.722 ± 0.356	0.88742 ± 0.00148	0.25288 ± 0.00393	3.000 ± 1.673

Table 7: Single-source transfer with clean data using Transformer.

Note that clipping does not increase the covering number of  $mH_d(W, L, B)$ . Using equation 10, equation 11 and equation 12 combined with Lemma B.1, we obtain

$$\log \mathcal{N}(\delta, \mathcal{G}_{d,p}(W, L, B; f_{\text{rep}}), \|\cdot\|_{L_\infty}) \lesssim W \log \left( \frac{LB^L(W+1)^L}{\delta} \right) + p \log \left( \frac{1}{\delta} \right).$$

This concludes the proof.  $\square$

## C More experimental results

In this section, we present additional results that complement the findings in Section 4.

### C.1 Experiments using clean pretrained data

Results using a CNN and a Transformer pretrained on clean data are shown in Table 6 and Table 7. REFINE performs comparably to LinearProb and Adapter, while consistently outperforming Distillation and NoTrans.

### C.2 Experiments with sub-optimal pretrained data using Transformer

Transformer results on CIFAR as the target domain under 80% label flips, domain mismatch, semantic confusion, and data imbalance are reported in Table 8, Table 9, Table 10, and Table 11, respectively. REFINE significantly outperforms all baselines under heavy label noise and remains comparable to or better than most competitive methods in the other settings, consistent with the CNN results.

Dataset	Model	Accuracy	AUC	F1	Min CAcc
CIFAR-10	NoTrans	45.168 ± 1.390	0.86783 ± 0.00277	0.43914 ± 0.01827	16.240 ± 4.517
	LinearProb	20.648 ± 0.443	0.68262 ± 0.00252	0.14104 ± 0.00828	0.000 ± 0.000
	Adapter	17.880 ± 0.733	0.66816 ± 0.00663	0.12481 ± 0.01110	0.000 ± 0.000
	Distillation	40.190 ± 0.569	0.84446 ± 0.00222	0.38269 ± 0.00682	8.000 ± 5.220
	REFINE	<b>45.526 ± 0.954</b>	<b>0.86940 ± 0.00465</b>	<b>0.44635 ± 0.01053</b>	<b>18.680 ± 4.966</b>
CIFAR-100	NoTrans	15.318 ± 0.333	<b>0.84489 ± 0.00210</b>	0.13584 ± 0.00411	0.000 ± 0.000
	LinearProb	6.700 ± 0.268	0.73766 ± 0.00112	0.03899 ± 0.00138	0.000 ± 0.000
	Adapter	6.544 ± 0.158	0.74048 ± 0.00113	0.03482 ± 0.00090	0.000 ± 0.000
	Distillation	11.826 ± 0.258	0.81299 ± 0.00268	0.08351 ± 0.00235	0.000 ± 0.000
	REFINE	<b>15.498 ± 0.785</b>	0.84372 ± 0.00412	<b>0.13781 ± 0.00671</b>	0.000 ± 0.000

Table 8: Single-source transfer with heavy label noise data using Transformer

Dataset	Model	Accuracy	AUC	F1	Min CAcc
CIFAR-10	NoTrans	44.374 ± 0.735	0.86277 ± 0.00345	0.43749 ± 0.00554	20.80 ± 4.863
	LinearProb	<b>46.044 ± 0.707</b>	<b>0.86428 ± 0.00150</b>	<b>0.45439 ± 0.00801</b>	23.46 ± 4.737
	Adapter	44.866 ± 0.553	0.85136 ± 0.00294	0.44445 ± 0.00588	26.74 ± 1.886
	REFINE	44.852 ± 0.379	0.85235 ± 0.00109	0.44736 ± 0.00346	<b>29.68 ± 1.779</b>
CIFAR-100	NoTrans	11.284 ± 0.524	0.80229 ± 0.00342	0.09841 ± 0.00327	0.000 ± 0.000
	LinearProb	13.322 ± 0.515	0.81855 ± 0.00153	0.11748 ± 0.00487	0.000 ± 0.000
	Adapter	12.636 ± 0.315	0.82665 ± 0.00058	0.10522 ± 0.00304	0.000 ± 0.000
	REFINE	<b>14.382 ± 0.540</b>	<b>0.82908 ± 0.00321</b>	<b>0.13288 ± 0.00386</b>	0.000 ± 0.000

Table 9: Single-source transfer under domain mismatches using Transformer.

Dataset	Model	Accuracy	AUC	F1	Min CAcc
CIFAR-10	NoTrans	45.36 ± 0.586	0.86624 ± 0.00333	0.44552 ± 0.00806	18.98 ± 7.493
	LinearProb	53.446 ± 0.436	0.90897 ± 0.00017	0.52589 ± 0.00778	26.28 ± 6.586
	Adapter	52.672 ± 0.328	0.90891 ± 0.00080	0.51948 ± 0.00502	30.84 ± 4.958
	Distillation	46.006 ± 1.107	0.87364 ± 0.00284	0.44345 ± 0.01425	14.00 ± 6.941
	REFINE	<b>54.616 ± 0.449</b>	<b>0.91340 ± 0.00104</b>	<b>0.54311 ± 0.00562</b>	<b>33.90 ± 3.338</b>
CIFAR-100	NoTrans	<b>16.236 ± 0.579</b>	<b>0.84709 ± 0.00362</b>	<b>0.14846 ± 0.00750</b>	0.000 ± 0.000
	LinearProb	11.884 ± 0.279	0.79501 ± 0.00157	0.10670 ± 0.00150	0.000 ± 0.000
	Adapter	11.172 ± 0.434	0.79356 ± 0.00270	0.09184 ± 0.00401	0.000 ± 0.000
	Distillation	15.006 ± 0.638	0.82658 ± 0.00278	0.12595 ± 0.00807	0.000 ± 0.000
	REFINE	14.938 ± 0.486	0.82823 ± 0.00256	0.14022 ± 0.00259	0.000 ± 0.000

Table 10: Single-source transfer with semantic confusion using Transformer

### C.3 Ablation Studies

To study the effect of fusion depth, we design a CNN with five fully connected layers after the convolutional blocks. Table 12 reports results on clean pretraining and CIFAR-10 with 80% label noise using three fusion configurations:  $L_1$  fuses at the last layer of  $h$ ,  $L_2$  at the last two, and  $L_3$  at the last three. Under clean pretraining, all variants perform similarly. With noisy pretraining,  $L_2$  outperforms  $L_1$ , which outperforms  $L_3$ , indicating a trade-off between representation richness and robustness.  $L_1$  may be preferred for its direct connection to the classification head and lower parameter cost.

To demonstrate that simply increasing parameter count in Adapter does not mitigate negative transfer, we perform an ablation on DVD→Electronics by scaling Adapter parameters by  $1\times$ ,  $25\times$ ,  $50\times$ ,  $100\times$ , and  $500\times$ . As shown in Figure 3, accuracy, AUC, and F1 do not improve, remaining significantly below both REFINE and NoTrans.

Dataset	Model	Accuracy	AUC	F1	Min CAcc
CIFAR-10	NoTrans	45.168 $\pm$ 1.390	0.86783 $\pm$ 0.00277	0.43914 $\pm$ 0.01827	16.240 $\pm$ 4.517
	LinearProb	<b>48.440 <math>\pm</math> 0.366</b>	<b>0.87494 <math>\pm</math> 0.00077</b>	<b>0.48049 <math>\pm</math> 0.00515</b>	25.940 $\pm$ 6.981
	Adapter	47.570 $\pm$ 0.273	0.86776 $\pm$ 0.00294	0.46894 $\pm$ 0.00453	25.260 $\pm$ 4.525
	Distillation	42.252 $\pm$ 0.633	0.86501 $\pm$ 0.00347	0.39960 $\pm$ 0.00513	3.860 $\pm$ 0.816
	REFINE	47.808 $\pm$ 0.231	0.86908 $\pm$ 0.00065	0.47551 $\pm$ 0.00262	<b>29.440 <math>\pm</math> 3.260</b>
CIFAR-100	NoTrans	15.430 $\pm$ 0.317	0.84741 $\pm$ 0.00245	0.13857 $\pm$ 0.00117	0.000 $\pm$ 0.000
	LinearProb	<b>25.818 <math>\pm</math> 0.280</b>	0.88772 $\pm$ 0.00102	<b>0.25292 <math>\pm</math> 0.00200</b>	3.600 $\pm$ 0.800
	Adapter	24.482 $\pm$ 0.322	0.88467 $\pm$ 0.00099	0.23198 $\pm$ 0.00271	0.600 $\pm$ 0.799
	Distillation	16.010 $\pm$ 0.127	0.87205 $\pm$ 0.00171	0.12515 $\pm$ 0.00207	0.000 $\pm$ 0.000
	REFINE	25.538 $\pm$ 0.430	<b>0.88791 <math>\pm</math> 0.00126</b>	0.25243 $\pm$ 0.00386	<b>4.800 <math>\pm</math> 0.748</b>

Table 11: Single-source transfer with imbalanced data using Transformer.

Noise Level	Model	Accuracy	AUC	F1	Min CAcc
Clean	REFINE <sub>L1</sub>	65.418 $\pm$ 0.293	0.93722 $\pm$ 0.00047	0.65444 $\pm$ 0.00259	47.18 $\pm$ 1.34
	REFINE <sub>L2</sub>	65.396 $\pm$ 0.160	0.93627 $\pm$ 0.00060	0.65420 $\pm$ 0.00153	47.52 $\pm$ 2.97
	REFINE <sub>L3</sub>	65.570 $\pm$ 0.281	0.93529 $\pm$ 0.00077	0.65578 $\pm$ 0.00226	47.84 $\pm$ 1.88
80% flips	REFINE <sub>L1</sub>	23.104 $\pm$ 1.473	0.76268 $\pm$ 0.02331	0.16728 $\pm$ 0.02708	0.62 $\pm$ 1.24
	REFINE <sub>L2</sub>	24.448 $\pm$ 0.763	0.78428 $\pm$ 0.00530	0.17164 $\pm$ 0.01048	0.00 $\pm$ 0.00
	REFINE <sub>L3</sub>	21.370 $\pm$ 0.764	0.76311 $\pm$ 0.00309	0.12896 $\pm$ 0.01516	0.00 $\pm$ 0.00

Table 12: Ablation Study of REFINE Performance with different fusion point on CIFAR-10.

In Figure 4, we show that REFINE scales effectively with an increasing number of external models. As we gradually concatenate features from up to 15 external models, we observe consistent improvements in accuracy, AUC, and F1 score. Owing to the design of REFINE, feature extraction can be implemented in parallel, enabling inference time to scale linearly with the number of models, but with only a modest slope.

#### C.4 Unweighted averaging is less robust

As previously noted, stacking methods such as unweighted averaging do not inherently support cross-domain or cross-task transfer. We further demonstrate that unweighted averaging can severely degrade performance when pretrained models fail, as evidenced on CIFAR-10 where unweighted averaging underperforms in the presence of corrupted pretrained models. In one experimental setup, we introduce class-dependent label noise to 2,000 pretraining examples by flipping 90% of class 1 to class 2, class 5 to class 4, and class 6 to class 7. As shown in Table 13, REFINE substantially improves performance, while

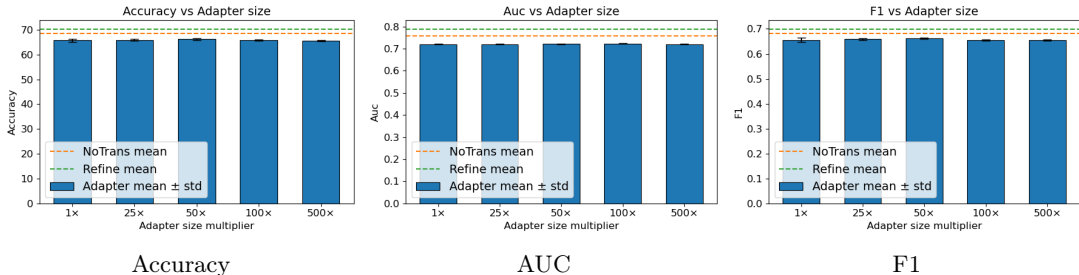


Figure 3: Performance of Adapter under varying parameter count multipliers.

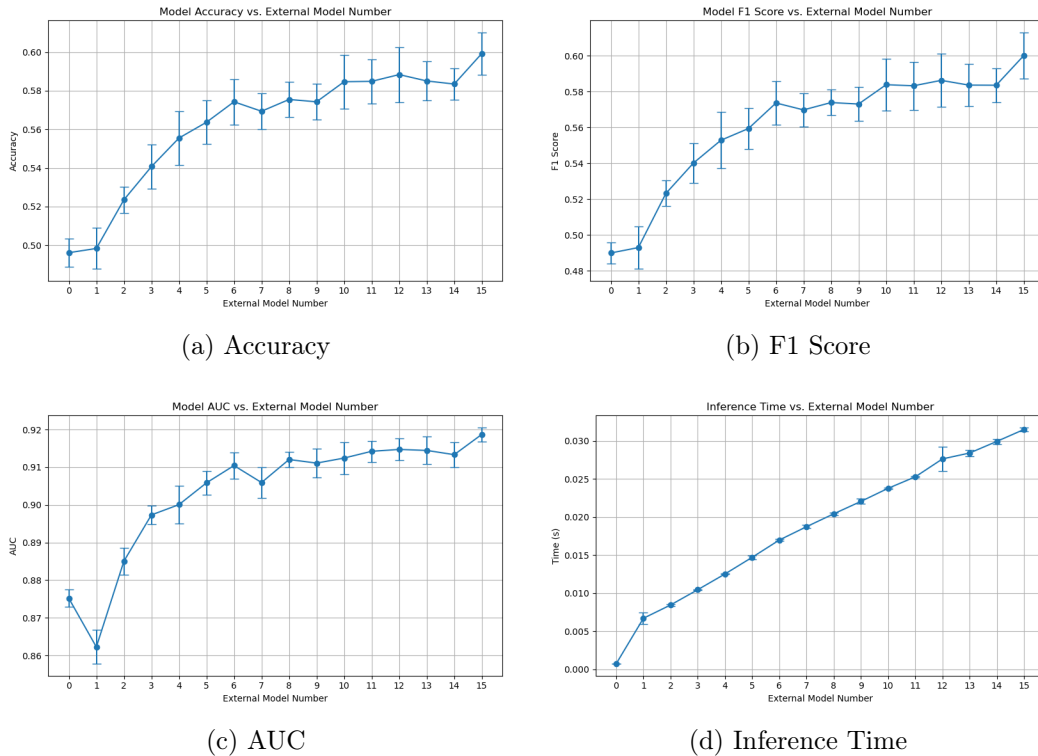


Figure 4: REFINe Scaling with Clean Sources

Table 13: Compare REFINe with UnweightedAvg under class-wise label flips.

Method	Accuracy	AUC	F1
NoTrans	41.82±1.44	0.852±0.007	0.405±0.017
Pretrain	32.29±1.61	0.825±0.008	0.276±0.015
REFINE	47.46±0.85	0.876±0.005	0.466±0.010
UnweightedAvg	40.77±1.58	0.868±0.003	0.373±0.024

Table 14: Compare REFINe with UnweightedAvg under label shift.

Method	Accuracy	AUC	F1
NoTrans	41.82±1.44	0.852±0.007	0.405±0.017
Pretrain	5.30±0.51	0.496±0.011	0.051±0.004
REFINE	48.74±1.12	0.883±0.005	0.479±0.012
UnweightedAvg	18.22±3.14	0.696±0.022	0.163±0.029

unweighted averaging exhibits noticeable degradation. In a separate setting, we permute class labels by randomly reassigning each class to a different label group, keeping the input features unchanged. As presented in Table 14, REFINe again outperforms unweighted averaging.

Table 15: Single-source transfer with clean pretrain data using MLP.

Dataset	Metric	Classifier					
		MLP1			MLP2		
		Raw	DirectAug	REFINE	Raw	DirectAug	REFINE
Adult	Accuracy	0.807 ± 0.008	0.831 ± 0.006	0.821 ± 0.004	0.800 ± 0.011	0.833 ± 0.005	0.814 ± 0.010
	AUC	0.832 ± 0.008	0.878 ± 0.006	0.852 ± 0.008	0.833 ± 0.010	0.883 ± 0.005	0.854 ± 0.008
	F1	0.547 ± 0.037	0.619 ± 0.015	0.595 ± 0.030	0.570 ± 0.028	0.627 ± 0.021	0.612 ± 0.021
Credit	Accuracy	0.723 ± 0.028	0.735 ± 0.017	0.740 ± 0.022	0.717 ± 0.027	0.732 ± 0.015	0.726 ± 0.020
	AUC	0.730 ± 0.024	0.738 ± 0.013	0.745 ± 0.018	0.725 ± 0.025	0.754 ± 0.020	0.736 ± 0.023
	F1	0.490 ± 0.043	0.524 ± 0.030	0.520 ± 0.038	0.515 ± 0.041	0.541 ± 0.030	0.535 ± 0.037
Diabetes	Accuracy	0.565 ± 0.015	0.573 ± 0.008	0.571 ± 0.008	0.561 ± 0.015	0.596 ± 0.007	0.572 ± 0.010
	AUC	0.582 ± 0.019	0.597 ± 0.008	0.591 ± 0.012	0.576 ± 0.018	0.626 ± 0.008	0.593 ± 0.013
	F1	0.505 ± 0.028	0.533 ± 0.014	0.523 ± 0.022	0.501 ± 0.029	0.534 ± 0.017	0.522 ± 0.027
Sim Binary	Accuracy	0.679 ± 0.014	0.748 ± 0.007	0.735 ± 0.010	0.684 ± 0.018	0.692 ± 0.077	0.715 ± 0.024
	AUC	0.694 ± 0.022	0.807 ± 0.008	0.779 ± 0.012	0.704 ± 0.026	0.736 ± 0.095	0.751 ± 0.037
	F1	0.397 ± 0.095	0.617 ± 0.020	0.599 ± 0.023	0.447 ± 0.092	0.563 ± 0.068	0.553 ± 0.084
Performance	Accuracy	0.684 ± 0.019	0.724 ± 0.011	0.711 ± 0.014	0.683 ± 0.018	0.668 ± 0.084	0.702 ± 0.022
	AUC	0.857 ± 0.011	0.878 ± 0.009	0.869 ± 0.009	0.858 ± 0.011	0.830 ± 0.070	0.865 ± 0.011
	F1	0.478 ± 0.025	0.557 ± 0.024	0.521 ± 0.029	0.478 ± 0.027	0.494 ± 0.090	0.507 ± 0.035
Sim Multi	Accuracy	0.577 ± 0.011	0.610 ± 0.006	0.596 ± 0.007	0.574 ± 0.011	0.550 ± 0.087	0.586 ± 0.013
	AUC	0.751 ± 0.010	0.786 ± 0.004	0.765 ± 0.007	0.749 ± 0.010	0.727 ± 0.084	0.757 ± 0.010
	F1	0.559 ± 0.013	0.595 ± 0.007	0.582 ± 0.008	0.557 ± 0.013	0.537 ± 0.083	0.572 ± 0.014

### C.5 REFINE over tabular data

We demonstrate that REFINE is also effective on tabular data and in data addition tasks. For tabular data, the concatenation is defined as  $X'_{\text{train}} = [X_{\text{train}}, \mathbf{P}]$ , where  $\mathbf{P} = f(X_{\text{train}})$ , with  $\mathbf{P} \in \mathbb{R}^{N \times K}$  and  $\sum_{k=1}^K P_{ik} = 1$  for each sample  $i$ . We evaluate on four binary classification datasets and two multiclass classification datasets. Each raw dataset contains  $K \times 100$  samples, where  $K$  is the number of classes. DirectAug refers to directly combining additional data with the Raw set to train the classifier. To assess model complexity, we design two MLP architectures: MLP1 with lower complexity, and MLP2 with a larger and more complex structure. As shown in Table 15, when additional data is clean, REFINE consistently improves all metrics and reduces variance. While DirectAug can perform better due to direct data merging, REFINE outperforms it in several cases, including Credit, Sim Binary, Performance, and Sim Multi. Label noise data retains covariates but has random labels. As shown in Table 16, DirectAug degrades performance, while REFINE maintains or slightly improves it. Besides label noise, we show that REFINE remains robust even when all features are replaced by standard Gaussian noise, as demonstrated in Table 17.

## D More Experimental Settings

We give more details about our experiments in this section for reproducibility. We use an NVIDIA A10G (Ampere) GPU with 23 GB of GDDR6 memory, running driver version 535.183.01 and CUDA 12.2. For semantic confusion in CIFAR-10 and CIFAR-100 experiments Tables 2 and 10, we have 4 and 47 pairs of related classes respectively, confusing them by flipping 50% to their counterpart and injecting white noise to the image attribute with sigma 0.2. In CIFAR-10 and CIFAR-100 imbalance Tables 3 and 11, we generate each imbalanced pre-training subset by first drawing 10 000 samples from the full training split using a fixed random seed (42): for CIFAR-10 we sample classes 0-9 with proportions 0.35,

Table 16: Single-source transfer with label noise pretrain data using MLP.

Dataset	Metric	Classifier					
		MLP1			MLP2		
		Raw	DirectAug	REFINE	Raw	DirectAug	REFINE
Adult	Accuracy	0.808 ± 0.007	0.615 ± 0.046	0.805 ± 0.008	0.800 ± 0.010	0.641 ± 0.052	0.791 ± 0.016
	AUC	0.834 ± 0.009	0.612 ± 0.051	0.832 ± 0.010	0.834 ± 0.013	0.639 ± 0.052	0.828 ± 0.014
	F1	0.549 ± 0.046	0.383 ± 0.039	0.555 ± 0.029	0.564 ± 0.032	0.395 ± 0.047	0.562 ± 0.027
Credit	Accuracy	0.723 ± 0.027	0.581 ± 0.035	0.705 ± 0.028	0.716 ± 0.027	0.599 ± 0.045	0.705 ± 0.028
	AUC	0.728 ± 0.027	0.578 ± 0.045	0.705 ± 0.028	0.720 ± 0.026	0.599 ± 0.045	0.687 ± 0.028
	F1	0.483 ± 0.049	0.417 ± 0.048	0.481 ± 0.035	0.512 ± 0.041	0.433 ± 0.041	0.493 ± 0.034
Diabetes	Accuracy	0.587 ± 0.007	0.516 ± 0.007	0.575 ± 0.006	0.614 ± 0.006	0.551 ± 0.016	0.609 ± 0.004
	AUC	0.580 ± 0.020	0.516 ± 0.014	0.554 ± 0.016	0.577 ± 0.017	0.585 ± 0.019	0.567 ± 0.020
	F1	0.503 ± 0.032	0.489 ± 0.025	0.498 ± 0.022	0.503 ± 0.026	0.483 ± 0.037	0.514 ± 0.025
Sim Binary	Accuracy	0.682 ± 0.015	0.666 ± 0.084	0.711 ± 0.013	0.682 ± 0.020	0.696 ± 0.079	0.696 ± 0.023
	AUC	0.697 ± 0.024	0.705 ± 0.103	0.742 ± 0.042	0.697 ± 0.024	0.705 ± 0.103	0.742 ± 0.042
	F1	0.414 ± 0.092	0.546 ± 0.075	0.529 ± 0.094	0.414 ± 0.092	0.546 ± 0.075	0.529 ± 0.094
Performance	Accuracy	0.682 ± 0.020	0.637 ± 0.088	0.696 ± 0.023	0.684 ± 0.018	0.650 ± 0.079	0.696 ± 0.023
	AUC	0.857 ± 0.011	0.805 ± 0.074	0.862 ± 0.011	0.859 ± 0.010	0.814 ± 0.068	0.863 ± 0.012
	F1	0.476 ± 0.028	0.464 ± 0.096	0.499 ± 0.036	0.480 ± 0.029	0.472 ± 0.088	0.500 ± 0.035
Sim Multi	Accuracy	0.596 ± 0.010	0.539 ± 0.127	0.603 ± 0.013	0.594 ± 0.010	0.539 ± 0.094	0.600 ± 0.013
	AUC	0.767 ± 0.008	0.712 ± 0.125	0.772 ± 0.010	0.765 ± 0.008	0.712 ± 0.091	0.769 ± 0.010
	F1	0.570 ± 0.014	0.525 ± 0.097	0.582 ± 0.017	0.570 ± 0.014	0.522 ± 0.092	0.580 ± 0.017

Table 17: Single-source transfer with feature noise pretrain data using MLP.

Dataset	Metric	MLP1			MLP2		
		Raw	DirectAug	ResAug	Raw	DirectAug	ResAug
		Adult	Accuracy	0.807 ± 0.007	0.776 ± 0.014	0.807 ± 0.005	0.797 ± 0.011
AUC	0.833 ± 0.010		0.721 ± 0.034	0.832 ± 0.010	0.831 ± 0.008	0.751 ± 0.020	0.832 ± 0.009
F1	0.547 ± 0.045		0.341 ± 0.090	0.549 ± 0.039	0.559 ± 0.032	0.302 ± 0.110	0.563 ± 0.035
Credit	Accuracy	0.722 ± 0.021	0.692 ± 0.027	0.722 ± 0.027	0.712 ± 0.028	0.693 ± 0.026	0.704 ± 0.028
	AUC	0.731 ± 0.023	0.664 ± 0.037	0.723 ± 0.028	0.724 ± 0.027	0.676 ± 0.031	0.708 ± 0.030
	F1	0.494 ± 0.033	0.404 ± 0.046	0.460 ± 0.043	0.507 ± 0.035	0.446 ± 0.044	0.486 ± 0.037
Diabetes	Accuracy	0.565 ± 0.014	0.522 ± 0.009	0.538 ± 0.012	0.560 ± 0.016	0.533 ± 0.014	0.547 ± 0.015
	AUC	0.581 ± 0.018	0.526 ± 0.011	0.552 ± 0.017	0.577 ± 0.020	0.536 ± 0.017	0.563 ± 0.018
	F1	0.503 ± 0.032	0.478 ± 0.021	0.492 ± 0.026	0.499 ± 0.025	0.457 ± 0.036	0.500 ± 0.023
Sim Binary	Accuracy	0.680 ± 0.014	0.619 ± 0.029	0.685 ± 0.016	0.690 ± 0.014	0.619 ± 0.029	0.686 ± 0.015
	AUC	0.695 ± 0.022	0.637 ± 0.028	0.709 ± 0.020	0.719 ± 0.019	0.630 ± 0.027	0.717 ± 0.016
	F1	0.397 ± 0.095	0.485 ± 0.020	0.487 ± 0.046	0.519 ± 0.043	0.471 ± 0.031	0.531 ± 0.025
Performance	Accuracy	0.684 ± 0.019	0.564 ± 0.018	0.675 ± 0.024	0.689 ± 0.017	0.581 ± 0.020	0.681 ± 0.018
	AUC	0.857 ± 0.011	0.743 ± 0.020	0.856 ± 0.012	0.863 ± 0.010	0.785 ± 0.018	0.859 ± 0.009
	F1	0.478 ± 0.025	0.303 ± 0.026	0.468 ± 0.031	0.482 ± 0.025	0.314 ± 0.031	0.472 ± 0.025
Sim Mult	Accuracy	0.577 ± 0.012	0.470 ± 0.017	0.574 ± 0.011	0.573 ± 0.012	0.477 ± 0.019	0.572 ± 0.013
	AUC	0.752 ± 0.010	0.627 ± 0.020	0.748 ± 0.011	0.749 ± 0.010	0.634 ± 0.022	0.746 ± 0.011
	F1	0.559 ± 0.013	0.420 ± 0.024	0.558 ± 0.012	0.558 ± 0.013	0.416 ± 0.028	0.557 ± 0.013

0.30, 0.10, 0.07, 0.06, 0.045, 0.03, 0.02, 0.015 and 0.01 (yielding 3 500, 3 000, 1 000, 700, 600, 450, 300, 200, 150 and 100 images per class); for CIFAR-100 we designate the first 10 classes as majority (400 images each) and the remaining 90 as minority (100 images each), truncating the collected indices to 10 000 samples in total.

We describe the experimental settings and hyperparameters for all experiments in Table 18 and Table 19. We ensure that the base model  $h$  is appropriate for the fine-tuning data and that the number of trainable parameters in REFINE is comparable to that of  $h$ , as

Dataset	Pretrain Model	Base Model	Pretrain Size	Fine-tune Size	Adapter Para (%)	REFINE Para (%)
CIFAR-CNN-related	CNN	CNN	10000	4000	5.46	4.88
CIFAR-TF-related	Transformer	Transformer	10000	4000	6.49	4.63
CIFAR-10→STL	CNN	CNN	10000	4000	5.46	4.88
Clipart→Sketch	ResNet18	ResNet10	3000	1000	1.36	44.2
USPS→MNIST	CNN	CNN	5000	100	5.46	4.88
Books→Kitchen	Transformer	Transformer	2000	400	2.25	96.58
DVD→Electronics	Transformer	Transformer	2000	400	2.25	96.58

Table 18: Dataset-specific settings for all experiments.

Dataset	Optimizer	LR	Pretrain Epochs	Fine-tune Epochs
CIFAR-CNN-related	SGD	0.01	60	30
CIFAR-TF-related	SGD	0.01	60	30
CIFAR-10→STL	SGD	0.01	60	30
Clipart→Sketch	SGD	0.01	20	20
USPS→MNIST	SGD	0.01	60	30
Books→Kitchen	SGD	0.01	20	20
DVD→Electronics	SGD	0.01	20	20

Table 19: Dataset-specific training hyperparameters across experiments

REFINE integrates  $h$  with external model features. REFINE may require more parameters than Adapter when the training task is highly demanding, as a sufficiently strong base model is necessary. However, simply increasing Adapter’s parameter count generally does not mitigate negative transfer in our setting, as evidenced in Figure 3 on DVD→Eletronics, where we increase the Adapter parameter count by factors of  $1\times$ ,  $25\times$ ,  $50\times$ ,  $100\times$ , and  $500\times$ . Therefore, we adopt a simple Adapter design following Houlsby et al. (2019) with  $1\times$  parameters. The parameter size in REFINE remains dependent on the user-specified  $h$ , balancing parameter efficiency and transfer safety, and can be kept small when the pretrained model is large and the target task is not overly difficult.